CAPITAL UNIVERSITY OF SCIENCE AND TECHNOLOGY, ISLAMABAD

Pharmacophore Modeling and Synthesis of Potential NF-κB Inhibitors as Anti-Alzheimer's Agents

by

Muhammad Amjad Sajjad

A thesis submitted in partial fulfillment for the degree of Master of Philosophy

in the

Faculty of Pharmacy
Department of Pharmaceutical Chemistry

2025

I dedicate this thesis to my loving and supportive teachers, family and friends, whose unwavering support has been crucial in helping me achieve my life goals.

CERTIFICATE OF APPROVAL

Pharmacophore Modeling and Synthesis of Potential NF-κB Inhibitors as Anti-Alzheimer's Agents

by

Muhammad Amjad Sajjad

(Registration No: MPH233022)

THESIS EXAMINING COMMITTEE

S. No.	Examiner	Name	Organization
(a)	External Examiner	Dr. Humaira Nadeem	RIU, Islamabad
(b)	Internal Examiner	Dr. Mahboob Alam	CUST, Islamabad

Dr. Reem
Thesis Supervisor
October, 2025

Dr. Reem
Head
Dept. of Pharmaceutical Chemistry
October, 2025

Dr. Muzaffar Abbas
Dean
Faculty of Pharmacy
October, 2025

Author's Declaration

I, **Muhammad Amjad Sajjad** hereby state that my MPhil thesis titled "**Pharmacophore Modeling and Synthesis of Potential NF-κB Inhibitors as Anti-Alzheimer's Agents**" is my own work and has not been submitted previously by me for taking any degree from Capital University of Science and Technology, Islamabad or anywhere else in the country/abroad.

At any time if my statement is found to be incorrect even after my graduation, the University has the right to withdraw my MPhil Degree.

(Muhammad Amjad Sajjad)

Registration No: MPH233022

Plagiarism Undertaking

I solemnly declare that research work presented in this thesis titled "**Pharmacophore Modeling and Synthesis of Potential NF-κB Inhibitors as Anti-Alzheimer's Agents**" is solely my research work with no significant contribution from any other person. Small contribution/help wherever taken has been duly acknowledged and that complete thesis has been written by me.

I understand the zero tolerance policy of the HEC and Capital University of Science and Technology towards plagiarism. Therefore, I as an author of the above titled thesis declare that no portion of my thesis has been plagiarized and any material used as reference is properly referred/cited.

I undertake that if I am found guilty of any formal plagiarism in the above titled thesis even after award of MPhil Degree, the University reserves the right to withdraw/revoke my MPhil degree and that HEC and the University have the right to publish my name on the HEC/University website on which names of students are placed who submitted plagiarized work.

(Muhammad Amjad Sajjad)

Registration No: MPH233022

Acknowledgement

In the name of **Allah**, the most gracious and the most merciful; and prayers and peace be upon **Muhammad**, His servant and messenger. First and foremost, I would like to acknowledge my limitless thanks to **Allah Almighty** and to his **last Prophet Muhammad (S.A.W)** without their guidance this work would have never become completed. I owe a deep gratitude to our University, **Capital University of Science & Technology (CUST)** for giving me such an opportunity to complete this work. A special thanks to the **Dean Dr. Muzaffar Abbas** for encouraging throughout the entire process. I would like to acknowledge and very grateful to my **Supervisor Dr. Reem** who has been always generous during all phases of the research and for all the valuable lessons that I learned during this period, I thank her from the bottom of my heart. I would like to express my heartfelt gratitude to Dr. Usman Shareef for his valuable guidance, encouragement, and constant support throughout my research journey. I am also sincerely thankful to Dr. Tariq Khan for his insightful suggestions and expert advice which helped shape the direction of this work.

I extend my warm thanks to my MPhil. classmates at Capital University of Science and Technology (CUST) for their support, cooperation, and friendship during this academic journey. I am equally grateful to my colleagues, especially Dr. Ahsan Ibrahim and Dr. Muhammad Arslan, at Shifa Tameer-e-Millat University for their encouragement, understanding, and positive environment throughout my MPhil. journey.

Finally, I want to express my wholehearted thanks to my **family**, specially **my parents** who have provided me generous support throughout my life and specially in doing my research. Because of their unconditional love, support and prayers, I have completed this thesis.

(Muhammad Amjad Sajjad)

Abstract

The combined application of pharmacophore modeling and synthetic organic chemistry has proven to be an efficient approach in identifying and developing potential NF-κB inhibitors. In this study, a systematic workflow was followed where ligand-based pharmacophore modeling, molecular docking, MM-GBSA scoring, molecular dynamics simulations, and in-silico ADMET analysis were used to select a promising lead compound. The identified molecule, named MAS-1, MAS-2 and MAS-3 was synthesized using a well-planned single pot reaction scheme. Its structural confirmation was carried out through FTIR and NMR analysis. Computational evaluations of MAS-3 revealed favorable drug-like properties including good solubility, high membrane permeability, low predicted toxicity, and the ability to cross the blood-brain barrier (BBB), a crucial factor for drugs intended to treat central nervous system disorders such as Alzheimer's disease. The compound also showed minimal interaction with key transporter proteins, supporting its potential for safe distribution and effectiveness. To support the in-silico findings, few in-vitro biological tests were performed. The DPPH antioxidant assay showed that MAS-3 outstands significant free radical scavenging activity, which is valuable considering the oxidative stress component in Alzheimer's pathogenesis. Moreover, brine shrimp lethality testing demonstrated a low toxicity profile, which further strengthens the compound's potential for future in-vivo studies. Overall, this study highlights the successful integration of computational drug design and lab-based synthesis and testing. The outcomes support MAS-1, MAS-2 and MAS-3 molecules as a promising NF-κB inhibitor with antioxidant properties and low toxicity, making it a suitable candidate for further biological evaluation. Future in-vitro and in-vivo assays, particularly enzyme inhibition and cell-based models, are essential to confirm its efficacy, mechanism, and therapeutic potential in managing neuroinflammatory diseases

Contents

List of Figures

List of Tables

Abbreviations

AD	Alzheimer's Disease
ADMET	Absorption, Distribution, Metabolism, Excretion and Toxicity
ALP	Alkaline Phosphatase
ALT	Alanine transaminase
APP	Amyloid Precursor Protein
AST	Aspartate Transaminase
AU-ROC	Area Under Receiving Operating Characteristics
A	Amyloid beta
BACE-1	Beta secretase
BBB	Blood Brain Barrier
BECROC	Binary Ensemble Averaged ROC
CADD	Computer Aided Drug Design
CYP	Cytochrome
DCM	Dichloromethane
EF 1%	Efficiency Factor 1%
FDA	Food and Drug Administration
FTIR	Fourier Transform Infrared
GGT	Gamma-glutamyl transferase
GH	Good of Hit List
HEK	Human Embryonic Kidney line
hERG	Human Ether-A-Go-Go
LDH	Lactate dehydrogenase
LID	Ligand interaction diagram
MD	Molecular Dynamics

MM-GBSA	Molecular Mechanics-Generalized Born Surface Area
NF-κB	Nuclear Factor kappa B
NFT	Neurofibrillary Tangles
NMDA	N-methyl-D-aspartate
OCT	Organic cation Transporter
P-gp	P-Glycoprotein
QSAR	Quantitative Structure Activity Relationship
RMSD	Root Mean Square Deviation
TD50	Toxic Dose 50
TLC	Thin layer chromatography
TSV	Tab Separated File
UGT	Uridine diphosphate (UDP)-glucuronosyltransferases
UTR	Untranslated terminal repeats
Vd	Volume of distribution

Chapter 1

Introduction

Developing new drugs, especially for complex brain disorders like Alzheimer's disease (AD), is a challenging and lengthy process. Traditional drug discovery often involves extensive trial-and-error experimentation, which is both time-consuming and incredibly expensive. Computer-Aided Drug Design (CADD) offers a more efficient and logical way to discover and improve new medicines, fundamentally transforming this landscape [1, 2]. By leveraging advanced computational power, CADD allows scientists to test many molecules virtually, predicting how they will interact with biological targets and assessing their drug-like properties long before any costly lab experiments are initiated. This approach not only significantly reduces the time and financial investment involved in drug development but also provides crucial, atomic-level insights into how molecules work at an early stage, thereby enhancing the rationality of the entire drug design process [3].

Pharmacophore modeling plays a central role within the framework of Computer-Aided Drug Design (CADD). This technique focuses on identifying the critical three-dimensional characteristics of a molecule that are essential for its biological activity. These features may include hydrogen bond donors or acceptors, aromatic rings, hydrophobic regions, or charged functional groups [4]. A pharmacophore model effectively shows the precise spatial arrangement of these features, which is needed for a molecule to interact optimally with a specific biological target, like the NF-κB protein in AD [5]. Pharmacophore modeling can be approached in two

primary ways. Ligand-based pharmacophore modeling analyzes a set of known active compounds to find common features, proving especially useful when the target protein's three-dimensional structure is unknown. This method assumes that molecules binding to the same target share a common set of interactions, and it seeks to define these common features by superimposing active compounds [6]. In contrast, structure-based pharmacophore modeling directly uses the known 3D structure of a protein-drug complex to identify these features, focusing on the specific interactions observed within the binding site, such as the geometry of the active site and the roles of key amino acid residues [7].

The wealth of known NF-κB inhibitors in databases like ChEMBL, coupled with their reported IC values, makes ligand-based pharmacophore modeling a particularly valuable tool for generating hypotheses that can then be validated through subsequent virtual screening and molecular docking to identify new potential drugs [8].

Following pharmacophore generation, molecular docking is a key computational method that predicts how a drug molecule will fit and bind within a target protein's active site [2]. This technique helps quickly identify promising compounds from large chemical libraries by evaluating their shape complementarity and non-covalent interactions (like hydrogen bonds, van der Waals forces, and electrostatic interactions) with the target. It also guides improvements to existing drug candidates by showing their exact binding modes, allowing medicinal chemists to make targeted modifications. However, traditional docking often assumes rigid protein structures, which can be a limitation. To go beyond these static predictions, molecular dynamics (MD) simulations provide a dynamic, atomic-level view of how proteins and drugs interact over time [9]. MD simulations reveal the natural flexibility of biological systems, including how their shapes change (e.g., through induced fit or conformational selection mechanisms) and how stable their binding is. This dynamic insight is crucial for understanding the true nature of molecular recognition and drug action, as proteins are not static entities but constantly moving[10]. Combining MD with pharmacophore modeling and docking leads to dynamic pharmacophores (which consider an ensemble of protein conformations)

and ensemble docking (where ligands are docked to multiple protein structures), offering more realistic views of drug-target interactions by accounting for protein flexibility [11, 12].

An essential part of rational drug design, particularly for drugs affecting the brain like those for AD, is the early evaluation of ADMET (Absorption, Distribution, Metabolism, Excretion, and Toxicity) properties [13]. Historically, poor ADMET profiles were a major reason for drug failures in late development stages, leading to significant financial and time losses. Identifying these issues only after substantial investment in clinical trials is extremely costly [13]. Computer-based ADMET prediction tools, using methods like QSAR, machine learning, and deep learning, allow researchers to filter out drug candidates with undesirable pharmacokinetic or safety issues early on. These tools can predict properties such as a compound's solubility, permeability across biological membranes, metabolic stability, and potential toxic effects [14]. This proactive approach ensures that potential drugs are not only effective but also drug-like and safe, and crucially, can cross the blood-brain barrier (BBB), which is vital for CNS drugs to reach their target in the brain.

The application of advanced computational methods is particularly relevant in addressing the pressing global health issue of Alzheimer's disease (AD). AD is a progressive neurodegenerative disorder characterized by memory loss, cognitive impairment, and behavioral changes, significantly affecting both patients and their caregivers. The hallmark pathological features of AD include the accumulation of amyloid-beta (Aβ) plaques outside neurons and neurofibrillary tangles formed by hyperphosphorylated tau protein within neurons. These abnormalities interfere with neural communication and eventually lead to widespread neuronal death [15]. While Aβ plaques and tau tangles are central to AD, growing evidence also points to the significant role of chronic neuroinflammation in the disease's progression [16]. In AD, the brain's immune cells, primarily microglia and astrocytes, become chronically active, releasing inflammatory chemicals (pro-inflammatory cytokines and chemokines) that worsen neuronal damage and accelerate neurodegeneration [17].

In this context, NF-κB (kappa-light-chain-enhancer of activated B cells), a key protein that controls immune and inflammatory responses, has emerged as a promising therapeutic target for AD as represented in figure 1.1. NF-κB becomes active in AD due to various stimuli, including Aβ accumulation and oxidative stress, leading to the production of inflammatory genes like tumor necrosis factor-alpha (TNF-α) and interleukins[5].

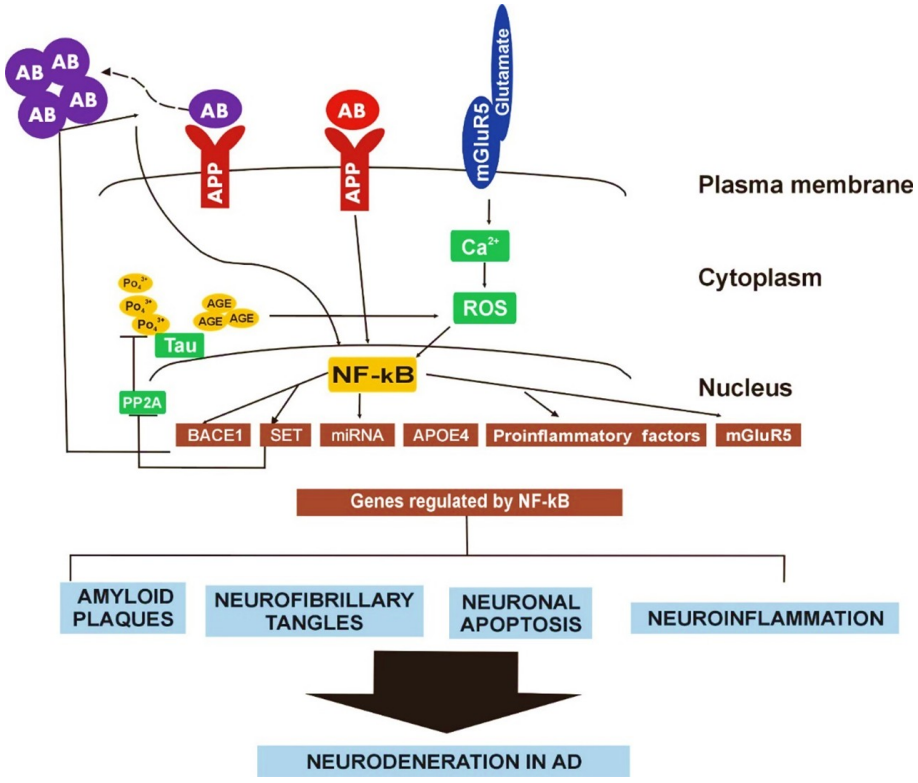

FIGURE 1.1: The central role of NF-κB in AD pathology. NF-κB facilitates the autocrine production of several factors that constitute AD pathology.

This creates a self-perpetuating cycle of inflammation that further harms neurons. Given NF-κB's central role in mediating neuroinflammation, targeting this pathway offers a compelling strategy to potentially reduce inflammation, protect neurons, and slow AD progression[18]. Therefore, computational methods, including pharmacophore modeling to identify key features for binding, molecular docking to predict interactions, MD simulations to understand dynamic behavior, and ADMET prediction to ensure drug-like properties, are being used strategically to find and improve new compounds that can modulate NF-κB activity, offering a rational path toward developing much-needed treatments for Alzheimer's disease.

1.1 Rationale of Study

Pharmacophore modeling is a well-established in-silico method that helps identify essential chemical features required for the interaction between a ligand and its target protein. It plays a crucial role in modern drug discovery by guiding the selection and design of new bioactive compounds. In neurodegenerative diseases like Alzheimer's, growing evidence highlights the involvement of chronic neuroinflammation, with nuclear factor kappa B (NF-κB) being a central player in this process. Abnormal activation of NF-κB has been strongly linked to the progression of Alzheimer's disease due to its regulation of pro-inflammatory genes and oxidative stress pathways.

Although NF-κB is a promising therapeutic target, its inhibition through ligand-based pharmacophore modeling remains underexplored. Previous studies, such as the one by Wolber et al., have identified NF-κB-related kinase inhibitors through ligand-based pharmacophore approaches, but only a few have proceeded to chemical synthesis or biological validation. Early screening tools like the *Artemia salina* lethality assay are valuable for predicting cytotoxicity and therapeutic relevance at a basic level.

1.2 Aim and Objectives

This study aims to apply pharmacophore modeling in combination with chemical synthesis to design and develop potential NF-κB inhibitors as therapeutic candidates for the treatment of Alzheimer's disease.

Specific objectives include:

• To carry out pharmacophore modeling aimed at identifying the essential chemical features responsible for the effective inhibition of NF-κB.

• To design new chemical compounds based on the developed pharmacophore model and assess their binding strength and selectivity toward the NF-κB target using molecular docking studies.

• To apply molecular dynamics simulations for analyzing the structural stability, flexibility, and detailed binding behavior of the protein-ligand complexes over time.

• To synthesize the most promising inhibitor(s) and confirm their structures through suitable analytical and characterization techniques.

Chapter 2

Literature Review

2.1 Introduction to Computer Aided Drug Design

The landscape of modern drug discovery is characterized by an increasing demand for efficiency, precision, and cost-effectiveness in the identification and development of novel therapeutic agents. In this challenging environment, computational approaches have emerged as indispensable tools, profoundly transforming the traditional paradigms of pharmaceutical research. Among these, pharmacophore modeling stands out as a particularly successful and expanding area within the broader field of computational drug design (CADD). A pharmacophore, at its essence, is an abstract description of the molecular features of a compound that are crucial for its biological activity. These features schematically illustrate the key elements of molecular recognition, typically represented in either two or three dimensions [12, 19].

The evolution of the pharmacophore concept itself, despite its origins preceding the advent of electronic computers, underscores its enduring utility and adaptability as a vital CADD tool [12]. The conceptual framework of a pharmacophore is

versatile enough to represent any atom or molecular group that exhibits properties relevant to molecular recognition, providing flexible language for describing essential interactions.

Furthermore, CADD methodologies are instrumental in generating critical information necessary for the development of Structure-Activity Relationships (SAR), which in turn facilitates the enhancement of molecules in terms of their desired biological activity and their Absorption, Distribution, Metabolism, and Excretion (ADME) properties [2].

Pharmacophores find extensive application in various computational strategies, including virtual screening, ADME-tox modeling, the prediction of side effects and off-target interactions, and target identification [20]. To further amplify their utility, pharmacophores are frequently integrated with molecular docking simulations, a combination that significantly enhances the effectiveness of virtual screening campaigns.

2.2 Historical Development of Pharmacophore Modeling

The concept of the pharmacophore, a cornerstone in rational drug design, has undergone a remarkable evolution, transitioning from an intuitive chemical idea to a sophisticated computational tool. This journey reflects the broader advancements in chemistry, biology, and computational science over more than a century. Pharmacophore modeling, a core concept in rational drug design, has evolved significantly over the last century. Initially, Paul Ehrlich in the early 1900s introduced the fundamental idea of specific molecular frameworks (pharmacon) carrying essential features (phoros) for biological activity, though the term "pharmacophore" itself gained prominence later [12, 21]. The modern era of pharmacophore formalization began with Peter Gund in 1977, who defined it as "a set of structural features in a molecule that is recognized at the receptor site and is responsible for that molecule's biological activity" [12, 22]. Lemont B. Kier further popularized

this concept from 1967, applying molecular orbital theory to describe common molecular features of ligands and map receptors. The first computer program, MOLPAT, was developed by Gund and colleagues in 1974 to automate pharmacophore identification [23, 24]. The 1980s and 1990s saw significant computational advancements driven by the emergence of 3D structural databases and software like CONCORD and CORINA. This led to automated pharmacophore generation tools such as Catalyst/HipHop, DISCO, and GASP, which helped identify key molecular features and handle conformational flexibility. HypoGen further advanced predictive modeling by correlating structure with activity. These tools were integrated into comprehensive molecular modeling packages like SYBYL and BIOVIA Discovery Studio, marking a crucial shift from 2D to 3D pharmacophore models [21, 24, 25]. The 2000s to the present define the modern era, characterized by the incorporation of machine learning (ML) and artificial intelligence (AI). ML and AI now analyze vast datasets to identify complex patterns and accurately predict compound activity. This integration enables high-throughput virtual screening of billions of molecules, significantly reducing the need for physical tests and accelerating drug discovery. A key development has been the emergence of dynamic pharmacophores, which account for protein flexibility. This continuous evolution, driven by technological advancements and multidisciplinary approaches, highlights pharmacophore modeling's increasing sophistication and its central role in modern drug design [26].

2.3 Pharmacophore Modeling

A pharmacophore represents the essential combination of structural and electronic features that a molecule must possess in order to bind effectively with a specific biological target, either to activate or inhibit a particular biological function. This concept has been formally recognized by the International Union of Pure and Applied Chemistry (IUPAC) since 1997. In pharmacophore modeling, researchers typically follow one of two main approaches.

TABLE 2.1: History of CADD and pharmacophore modeling

Year	Contribution	Key Researchers/Tools	Impact
Early 1900s	Introduction of the pharmacophore concept (as molecular framework for activity)	Paul Ehrlich	Laid conceptual groundwork for understanding drug-receptor interactions [23].
1967-1971	Popularization of the modern pharmacophore concept (abstract features in 3D)	Lemont B. Kier	Shifted focus to 3D spatial relationships, applied molecular orbital theory to receptor mapping [27].
1974	Development of the first computer program for pharmacophore patterns	MOLPAT (Gund, Wipke, Langridge)	Initial automation of pharmacophore identification [24].
1977	Modern, widely accepted definition of pharmacophore	Peter Gund	Formalized the definition of a pharmacophore as a set of structural features recognized at the receptor [12].

Continuous on next page

Table 2.1: Continuous from previous page

Year	Contribution	Key Researchers/Tools	Impact
1987-1989	Emergence of rapid 3D structure generation software	CONCORD, CORINA, AIMB, WIZARD	Enabled conversion of 2D databases to 3D, crucial for 3D-searching [12].
Late 1989-Early 1990s	Release of first commercial 3D searching/pharmacophore systems	MACCS-3D, ChemDBS-3D, UNITY, Catalyst	Revolutionized 3D database mining and query generation in pharmaceutical industry [28].
Early 1990s	Development of specialized automated pharmacophore software	DISCO, HipHop, GASP, HypoGen	Provided tools for automated pharmacophore generation, alignment, and activity correlation [29].
2000s-Present	Incorporation of Machine Learning/AI and Dynamic Pharmacophores	Various ML/AI algorithms, MD simulation software	Enabled analysis of large datasets, predictive modeling, and accounting for protein flexibility [10].

The first is the ligand based method, where multiple active compounds are analyzed together to identify common chemical features responsible for their activity. The second is the structure based method, which focuses on studying how molecules interact directly with the three dimensional structure of the target protein to determine the critical binding interactions. [30].

Pharmacophore modeling serves as a highly valuable technique throughout various phases of drug discovery. It is especially useful in creating novel molecules from the ground up (de novo design), as well as in the modification and enhancement of existing drug candidates to improve their biological performance (lead optimization).

This approach also plays a central role in virtual screening, where extensive chemical databases are explored to identify promising bioactive compounds. Moreover, pharmacophore modeling supports the development of multi target drugs, which are designed to interact with more than one biological receptor or pathway.

With continuous advancements in computational tools and methodologies over the last twenty years, the field has witnessed the emergence of automated and highly efficient pharmacophore modeling systems, making it more accessible and impactful in modern pharmaceutical research [31]. Several recent achievements have clearly demonstrated the effectiveness of pharmacophore modeling in accelerating the drug discovery process.

These success stories underline its value in identifying promising candidates more efficiently and cost effectively compared to traditional methods. Despite these advancements, pharmacophore based approaches still face certain limitations. One of the major challenges lies in overcoming the high financial burden associated with bringing new drug candidates from concept to clinic. Reducing these costs remains a significant barrier to fully realizing the potential of pharmacophore modeling in modern drug development [11, 32].

Pharmacophore models, central to computational drug design, are categorized by the information used for their generation: ligand structures, target protein structures, or a combination incorporating dynamic considerations. Each type

offers distinct advantages, making them suitable for various drug discovery stages based on data availability.

2.3.1 Ligand-Based Pharmacophores

Ligand-based pharmacophore modeling (LBP) is crucial when target protein structural information is unavailable. It derives models exclusively from known active ligand structures, based on the premise that molecules interacting with the same target share common activity-responsible structural features [33]. LBP model generation involves selecting a diverse training set of active and inactive compounds for discrimination. Low-energy conformations are then generated for each molecule to capture probable bioactive forms. These are superimposed to identify common functional groups, with the best fit across active molecules representing the active conformation. This superimposition is abstracted into pharmacophore elements like aromatic ring or hydrogen-bond donor/acceptor. Common methods include feature alignment and QSAR modeling, supported by tools such as LigandScout, Phase, and MOE [34, 35].

2.3.2 Structure-Based Pharmacophores

Structure-based pharmacophore modeling (SBP) utilizes explicit three-dimensional target protein structural information, typically from X-ray crystallography or NMR spectroscopy. SBP models are constructed directly from protein active site features, describing key ligand interactions. This method is advantageous when the target structure is known with high confidence [36].

SBP methodology involves detailed analysis of binding site chemical properties to identify crucial interaction points (e.g., hydrogen bond donors/acceptors, hydrophobic regions) for pharmacophore model construction [12]. Tools like LigandScout automate query construction from PDB files based on observed interactions. A recent advancement, the apo2ph4 workflow, derives high-quality models solely

from receptor 3D structure, even without known ligands. Specialized SBP software, including AutoLigand and Pocket v.2, identifies binding sites and derives models from protein-ligand complexes with minimal manual intervention [4, 19].

2.3.3 Hybrid Pharmacophores

Hybrid pharmacophore modeling synergistically combines ligand-based and structure-based drug design approaches [32]. This integrated methodology offers a more comprehensive understanding of intricate ligand-protein interactions, leading to more potent and selective drug candidates. Hybrid pharmacophores are particularly valuable for complex biological targets or when structural data is limited, leveraging both known ligand information and available structural insights to enhance model accuracy and predictive power, overcoming individual method limitations[37].

2.3.4 Dynamic Pharmacophores

Dynamic pharmacophores represent a crucial advancement, moving beyond static molecular interaction representations by explicitly incorporating protein and ligand flexibility, often using molecular dynamics (MD) simulations. This evolution stems from recognizing that proteins are dynamic systems undergoing conformational changes (induced-fit) or selecting pre-existing states (conformational selection) upon ligand binding.

A single, fixed protein conformation is often inadequate to accurately represent complex ligand binding[38]. Dynamic pharmacophore models are constructed by analyzing MD simulation snapshots, capturing continuous motion and conformational variability of the protein-ligand system. This identifies conserved binding regions despite active site flexibility. Increased conformational sampling via MD consistently improves pharmacophore models, emphasizing the importance of integrating target flexibility in structure-based drug design.

TABLE 2.3: Comparison between ligand-based, structure-based, hybrid, and dynamic pharmacophore modeling.

Type	Data Source	Strengths	Limitations	Key Tools
Ligand-Based	Set of active ligands, often with inactive compounds for discrimination	Useful when target structure is unknown; identifies common features essential for activity; good for Structure-Activity Relationship (SAR) studies.	Assumes common features are essential; dependent on pre-computed conformation databases; lacks explicit protein interaction information.	LigandScout, Phase, MOE [39]
Structure-Based	Protein 3D structure (e.g., X-ray, NMR), often from protein-ligand complexes	Direct optimization to match binding site; high accuracy when target structure is known; predicts binding modes based on explicit interactions.	Requires known target structure; may not fully account for protein flexibility.	AutoLigand, Pocket v.2 [34]

Continuous on next page

Table 2.2: Continued from Previous Page

Type	Data Source	Strengths	Limitations	Key Tools
Hybrid	Combination of ligand structures and protein structural data	Enhanced accuracy and comprehensiveness; provides a more complete understanding of interactions; useful for complex targets with limited structural data.	It can be more complex to implement and validate due to diverse data integration	Often implemented within comprehensive suites like Discovery Studio [28]
Dynamic	Molecular dynamics (MD) simulations, ensemble of protein conformations	Accounts for protein and ligand flexibility; relevant for induced fit and allosteric binding sites; improved accuracy in dynamic systems.	Computationally intensive; requires extensive MD simulations and specialized analysis.	Integrated MD software (e.g., AMBER, Phase, GROMACS) with pharmacophore analysis tools [40]

This type is highly relevant for designing drugs targeting flexible or allosteric binding sites and induced-fit effects, enabling more realistic exploration of complex interactions [41, 42]. This progression highlights a continuous pursuit of methods that more accurately reflect intricate molecular recognition processes, adapting to and leveraging experimental and computational advancements[43].

2.4 Ligand-based Pharmacophore Modeling

Ligand-based drug discovery (LBDD) is a fundamental computational approach that complements structure-based methods, particularly when detailed structural information about the molecular target is unavailable. This methodology leverages the wealth of knowledge derived from existing ligands to design and optimize new drug candidates. At its core, LBDD operates on the principle that molecules with similar chemical structures are likely to exhibit similar biological activities, often referred to as the "similarity-property principle". This principle underpins the entire LBDD paradigm, allowing researchers to predict how novel molecules might interact with a target based on the behavior of known binders [6, 44].

LBDD is an iterative process that correlates the biological activity of compounds with their chemical structure, thereby establishing Structure-Activity Relationships (SAR)[45]. The primary aim is to identify compounds optimized for a given biological activity, often through a cycle of chemical synthesis and bioactivity screening. The workflow for LBDD typically involves a series of interconnected steps, beginning with the careful selection of ligands. This initial phase involves identifying a comprehensive set of known active ligands, and ideally, inactive compounds, to provide a robust dataset for model training [46].

Following ligand selection, the next critical step is features identification. This involves analyzing the structural and chemical properties of these ligands to pinpoint the essential features responsible for their biological activity. Pharmacophore modeling is a key technique employed here, as it allows for the abstraction of these

features into a predictive model [47]. Subsequently, a predictive model is generated, which can take various forms, including pharmacophore models or Quantitative Structure-Activity Relationship (QSAR) models. These models are built upon the identified features and their established relationship to biological activity [47]. The final and often most impactful step in the computational workflow is virtual screening. Here, the generated model is utilized as a query to rapidly screen large compound libraries, aiming to identify potential "hits" that are predicted to exhibit the desired biological activity [48].

2.4.1 Pharmacophore-Based Virtual Screening

Pharmacophore-based virtual screening (VS) is a cornerstone application within LBDD. Its primary purpose is to efficiently filter vast chemical libraries, prioritizing molecules that are most likely to be active against a specific target. This computational filtering significantly reduces the need for extensive and costly experimental high-throughput screening (HTS), thereby saving considerable time and resources in the early stages of drug discovery by quickly identifying promising compounds for further laboratory testing [49].

The process of hit prioritization in pharmacophore-based VS relies on scoring functions that evaluate how well a candidate molecule "fits" or matches the pharmacophore features of the query model. This fit is often quantified as a Root Mean Square Deviation (RMSD) value, where a lower RMSD indicates a better match[50]. Scoring functions can incorporate various geometric and chemical features, including hydrogen bond acceptors/donors, hydrophobic groups, and charged groups, to assess and rank the potential binding geometries of compounds [47].

LBDD has demonstrated considerable success across various drug discovery projects. Notable examples include its application in the design of novel HIV protease inhibitors and the development of selective COX-2 inhibitors [51]. In the realm of G protein-coupled receptors (GPCRs), LBDD methods, particularly 3D-QSAR, have proven invaluable for rationalizing the activity of known ligands and

identifying novel ones. This is especially significant given the persistent challenges in obtaining experimental structural information for many GPCRs, which are notoriously difficult to crystallize [52]. Pharmacophore-based design, for instance, has been successfully employed to identify non-peptidic ligands for peptide-binding GPCRs, addressing issues like poor bioavailability and metabolic instability often associated with peptide ligands. Furthermore, LBDD, frequently augmented by machine learning (ML) techniques, is a common approach in kinase drug discovery. The FDA has approved numerous small molecule protein kinase inhibitors, many of which have benefited from LBDD in their discovery and optimization phases, leveraging the underlying similarity-property principle [6, 36].

Despite its successes, LBDD is not without its limitations. A primary constraint is its inherent reliance on structural information about known ligands, which means it cannot be applied when no active compounds are known for a target. Moreover, LBDD models may not always accurately predict the biological activity of novel molecules, necessitating rigorous experimental validation of any identified compounds [53]. A significant challenge in LBDD is scaffold hopping, which refers to the identification of bioactive compounds that are structurally distinct from known active compounds but retain similar biological activity. The activity landscape of molecules is often non-linear, meaning that even small structural changes can lead to large and unpredictable shifts in biological activity. This inherent complexity complicates the application of simple similarity metrics for identifying novel scaffolds. Therefore, while LBDD excels at refining existing lead compounds (lead optimization), it faces inherent difficulties in true de novo design or radical scaffold changes without extensive experimental validation [54].

The reliance of LBDD on the similarity-property principle is both its greatest strength and its most significant limitation. While this principle allows for efficient identification of analogous compounds and refinement of existing leads, it becomes a hurdle when the goal is to discover entirely novel chemical scaffolds or circumvent intellectual property issues [55]. The observation that small structural changes can lead to large shifts in biological activity directly challenges the simplicity of the similarity principle, indicating that molecular interactions are far more complex

than a simple linear relationship might suggest. This suggests that while LBDD is highly effective for lead optimization within a known chemical series, achieving true structural novelty often requires integrating LBDD with other, more exploratory computational methods or accepting a higher rate of failure for novel chemotypes [19].

Furthermore, LBDD maintains its enduring relevance despite the increasing advancements in structural biology. Even with the proliferation of protein structures, LBDD remains crucial, particularly for challenging targets like GPCRs where obtaining high-resolution structural information is still difficult or impossible. This highlights that many biological targets continue to lack experimentally determined structures, making LBDD a practical necessity for "orphan receptors" and other difficult-to-crystallize proteins [56]. The continued reliance on ligand-based approaches, driven by the experimental difficulty in obtaining target structures, underscores the complementary nature of LBDD and structure-based drug design. Rather than one method replacing the other, they serve as indispensable tools in different contexts, collectively advancing the field of drug discovery [7].

2.5 Molecular Docking

Molecular docking is a widely used computational method that helps predict how a small molecule, known as a ligand, fits and interacts with a specific biological target, typically a protein. This technique simulates the binding process to understand how well the ligand can attach to the receptor's active site. By applying different scoring functions, molecular docking evaluates and ranks the binding strength of various ligands, providing insights into their potential effectiveness as drug candidates [57]. Effective ligand binding within a target's active site depends on two essential factors:

• Exploring multiple binding orientations and conformations to consider all possible ways the ligand can fit into the active site.

• Accurately predicting the binding strength for each orientation to determine which pose offers the most stable and effective interaction [58].

Molecular docking is generally categorized into two types: flexible-ligand and flexible-protein docking. Flexible ligand docking focuses on the ligand's ability to adopt various shapes using simulation or systematic methods. In contrast, flexible-protein docking accounts for the dynamic nature of the protein target, often using Monte Carlo or molecular dynamics simulations to model changes in the binding site during interaction [59].

2.6 Molecular Dynamic Simulation

In drug development, molecular dynamics (MD) simulations serve as a vital computational tool for understanding the behavior and interactions of molecules at the atomic level. By applying principles of physics, MD simulations track the movement of atoms and molecules over time, providing detailed insights into their stability, flexibility, and dynamic behavior in different environments [9]. Molecular dynamics (MD) simulations have gained widespread popularity due to their unique advantages.

They allow researchers to track the exact positions and movements of all particles in a system with remarkable detail at every time step—something that experimental methods often struggle to capture. One of the key strengths of MD simulations is the ability to maintain full control over system parameters, which can be easily adjusted to explore various conditions and behaviors with precision[60].

Due to their ability to reveal detailed atomic-level interactions, molecular dynamics (MD) simulations play a key role in structure-based drug development. They are especially useful for studying essential processes such as ligand binding and unbinding, as well as the dynamic conformational changes within receptors. These subtle yet critical insights, often beyond the reach of experimental techniques, can be captured with high precision through MD simulations [40].

2.7 Overview of AD

Alzheimer's disease (AD) is a chronic and progressive neurodegenerative disorder, recognized as the most common cause of dementia, accounting for nearly 60–70% of global cases [60]. Its prevalence increases sharply with advancing age, particularly among individuals over the age of 65, where approximately 11% are affected [62]. Clinically, AD presents with a gradual decline in memory, cognitive reasoning, and behavioral functioning. However, early diagnosis remains a challenge, as some individuals report memory concerns despite showing no measurable cognitive deficits, a condition often described as the "worried well" [61]. The diagnostic complexity is further heightened by the symptomatic overlap between AD and other neurodegenerative disorders such as frontotemporal dementia and Lewy body dementia, making differential diagnosis difficult in early stages. Several modifiable risk factors have also been implicated in the onset and progression of AD. Cardiometabolic disorders—such as hypertension, type 2 diabetes, and obesity have been strongly associated with a higher risk of cognitive decline. These conditions are believed to contribute to neurodegeneration through mechanisms involving insulin resistance, chronic inflammation, and vascular dysfunction [61]. From a pathological standpoint, AD is characterized by two hallmark features: the accumulation of amyloid-beta (Aβ) plaques in the extracellular space and the formation of intracellular neurofibrillary tangles composed of hyperphosphorylated tau protein. These abnormal protein deposits interfere with neuronal signaling and ultimately lead to synaptic dysfunction and neuronal death [62]. Importantly, these pathological changes often begin many years before the clinical onset of symptoms, underscoring the need for early identification and intervention strategies to slow or halt disease progression [63].

2.8 Epidemiology

Alzheimer's disease (AD) is a progressive neurodegenerative condition and the leading cause of dementia worldwide, accounting for approximately 60–70% of all

cases [64]. Its global prevalence is steadily increasing, primarily driven by aging populations, with projections suggesting a substantial rise in AD cases by the year 2050 [65].

In Pakistan, this trend closely follows global patterns. Currently, it is estimated that around 400,000 individuals in the country are living with dementia—a number expected to rise significantly in the coming decades [66]. Several contributing factors have been identified, including increased life expectancy, rapid urbanization, and shifts in lifestyle that have led to a greater incidence of cardiometabolic risk factors such as hypertension, type 2 diabetes, and obesity. Additionally, societal attitudes and limited public awareness regarding dementia often result in delayed diagnosis and inadequate care, further compounding the challenges associated with managing AD in the local context [67].

2.9 Economic Impact

Alzheimer's disease (AD) presents a growing economic challenge on a global scale, encompassing not only direct medical expenses and long-term social care but also a significant contribution from informal caregiving. The total worldwide cost of AD and related dementias is projected to reach nearly $14.5 trillion by 2050, representing approximately 0.42% of the global annual GDP [68]. This rising financial burden is closely tied to the increasing prevalence of the disease and the continued absence of a definitive cure. A major share of these costs arises from informal, unpaid caregiving. In high-income countries, informal care accounts for nearly 60% of total dementia-related expenditures, while in low- and middle-income nations, such as Pakistan, this figure can rise to as much as 85% [67]. This heavy dependence on family caregivers reflects both the societal gaps in professional support services and the immense personal and economic pressure placed on affected households. In Pakistan, managing AD is further complicated by limited healthcare infrastructure and the scarcity of specialized geriatric care facilities. With an estimated 400,000 individuals currently living with dementia, a number expected to grow rapidly due to demographic trends, the financial impact

is largely absorbed by families. In the absence of formal support systems, out-of-pocket health expenses, along with income losses related to caregiving duties, contribute significantly to the overall economic strain [69].

2.10 Molecular Mechanisms Driving AD

Alzheimer's disease (AD) is a complex, multifactorial neurodegenerative condition, primarily marked by a gradual decline in cognitive abilities and memory. Its pathogenesis involves a network of molecular and cellular events that contribute to neuronal dysfunction and brain atrophy over time. One of the most widely accepted explanations is the amyloid cascade hypothesis, which suggests that the abnormal accumulation of amyloid-beta (Aβ) peptides plays a central role in initiating the disease process. These peptides are generated through the improper cleavage of amyloid precursor protein (APP) by the enzymes β-secretase and -secretase.

The resulting Aβ fragments aggregate to form insoluble extracellular plaques, which interfere with synaptic communication, exert neurotoxic effects, and trigger a cascade of neurodegenerative changes within the brain. [70]. Alongside amyloid deposition, the hyperphosphorylation of tau proteins leads to the development of intracellular neurofibrillary tangles (NFTs), which disrupt neuronal architecture and contribute to cell death. Neuroinflammation, driven by the activation of microglia and astrocytes, plays a significant role in accelerating neurodegeneration through the sustained release of pro-inflammatory cytokines and reactive oxygen species (ROS) [71]. In parallel, mitochondrial dysfunction and elevated oxidative stress impair neuronal energy production, rendering neurons more susceptible to damage and degeneration [72].

Another key feature is the cholinergic deficit, characterized by the degeneration of cholinergic neurons in the basal forebrain, which correlates closely with the severity of cognitive impairment observed in AD patients [73].

Additionally, vascular abnormalities, such as cerebral amyloid angiopathy and compromised blood-brain barrier (BBB) integrity, contribute to disease progression by reducing cerebral perfusion and allowing harmful substances to enter the brain environment [74].

Recent studies also point toward the role of gut microbiota imbalance, or dysbiosis, in influencing brain inflammation and amyloid pathology, suggesting a complex gut-brain axis interaction in the pathogenesis of AD [75]. Collectively, these overlapping mechanisms highlight the multifactorial nature of AD and emphasize the importance of pursuing integrated therapeutic strategies that target multiple pathological pathways.

2.11 Neuroinflammation

Neuroinflammation has emerged as a third major hallmark of Alzheimer's disease (AD), alongside amyloid plaques and tau tangles. Although inflammation in the brain is initially protective—aimed at removing harmful agents and clearing cellular debris—its persistent and uncontrolled activation in AD becomes harmful. Rather than resolving pathology, chronic neuroinflammation contributes to the progression of the disease by accelerating amyloid-beta (Aβ) and tau pathology, promoting neuronal injury, and facilitating synaptic loss. Two key cellular players in this process are microglia and astrocytes. Microglia, the brain's resident immune cells, respond to pathological triggers such as Aβ deposits and hyperphosphorylated tau [15]. In early stages, they may help clear Aβ, but with prolonged stimulation, microglia undergo a shift toward a pro-inflammatory (M1-like) state.

In this dysfunctional state, they release elevated levels of inflammatory cytokines—such as interleukin-1β (IL-1β), interleukin-6 (IL-6), and tumor necrosis factor-alpha (TNF-α)—along with reactive oxygen species (ROS), which further damage neurons and promote disease progression [76].

Astrocytes, another type of glial cell, also become reactive in response to Aβ, contributing to the inflammatory environment. Their dysfunction can disrupt blood-brain barrier (BBB) integrity and amplify local immune responses.

Several critical signaling pathways regulate this inflammatory cascade, including the NLRP3 inflammasome and the nuclear factor kappa-light-chain-enhancer of activated B cells (NF κ B) pathway. Aβ has been shown to activate the NLRP3 inflammasome, which triggers the production of pro-inflammatory cytokines. Meanwhile, NF κB a key transcription factor activated by Aβ, lipopolysaccharides (LPS), and ROS—promotes the expression of inflammatory genes and microRNAs involved in amyloidogenesis, glial activation, synaptic dysfunction, and neuronal death. This persistent inflammatory state not only causes further neuronal injury but also amplifies Aβ accumulation and tau spreading, creating a vicious cycle that continuously worsens the neurodegenerative process [15].

2.12 Link Between Neuroinflammation and NF-κB

The Nuclear factor kappa-light-chain-enhancer of activated B cells (NF-κB) signaling pathway plays a critical and central role in regulating the neuroinflammatory response associated with Alzheimer's disease (AD). As a key DNA-binding transcription factor, NF-κB influences multiple cellular processes relevant to AD pathology, including immune activation, inflammatory signaling, cell survival, and differentiation. Its dysregulation is increasingly recognized as a major contributor to the chronic inflammatory environment observed in the AD brain, making it a focal point for therapeutic exploration [18].

2.12.1 Role of Amyloid-beta (Aβ) Peptides

The NF-κB signaling pathway serves as a crucial mediator of the neuroinflammatory processes implicated in Alzheimer's disease (AD). As a pivotal transcription

factor with DNA-binding capabilities, NF-κ B governs several cellular activities, including immune response regulation, pro-inflammatory gene expression, cellular differentiation, and cell survival. In the context of AD, the persistent activation or dysregulation of NF-κB has been strongly linked to the sustained inflammatory state in the brain. This has positioned the pathway as a promising therapeutic target for efforts aimed at mitigating neuroinflammation and slowing disease progression [18, 76].

2.12.2 NF-κB Dual Behavior in AD Progression

The involvement of NF-κB in Alzheimer's disease (AD) is multifaceted, exhibiting cell-type-dependent roles that can be either neuroprotective or neurotoxic. In healthy neurons, NF-κB contributes to essential physiological functions, including neurotransmission, synaptic plasticity, learning, memory consolidation, and even DNA repair.

It also plays a protective role by inhibiting apoptosis and necroptosis, thus supporting neuronal survival. However, in the context of AD pathology, this balance shifts.

There is often a decline in neuronal NF-κB activity, paralleled by a marked increase in NF-κB activation within glial cells, particularly astrocytes and microglia. This heightened glial NF-κB signaling contributes to chronic neuroinflammation and promotes neuronal damage.

Neuropathological evidence indicates an accumulation of nuclear phosphorylated RELA (a transcriptionally active NF-κB subunit) in astrocytes from AD brains, suggesting a sustained TNFR-mediated NF-κB activation. This activation pattern reflects a pro-inflammatory shift that is detrimental to neuronal health and may drive disease progression as illustrated in the figure [64].

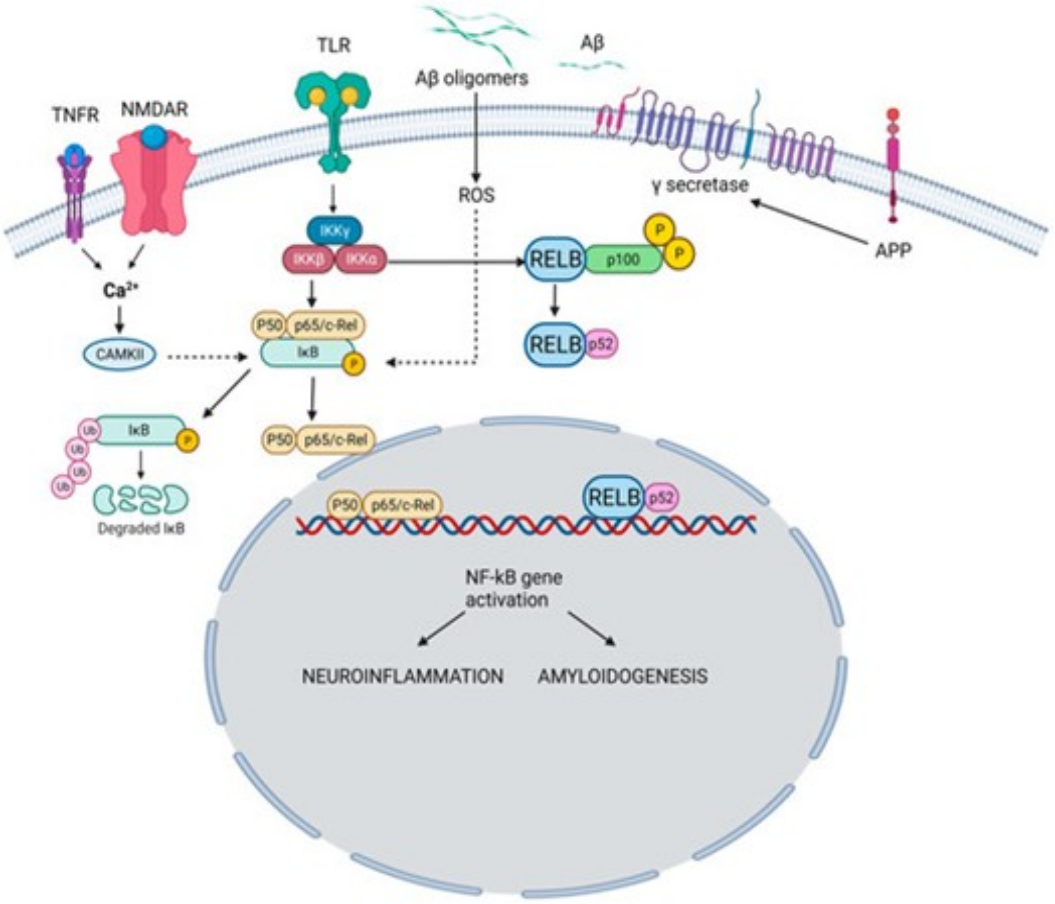

FIGURE 2.1: Role of NF-κB in pathogenesis of Alzheimer's disease (AD)

2.12.3 NF-κB's Direct and Indirect Contributions to AD Pathogenesis

NF-κB plays a multifaceted role in the pathogenesis of Alzheimer's disease (AD), contributing both directly and indirectly to neurodegenerative processes. It is directly activated by pathological features of AD and indirectly sustains disease progression through regulation of various inflammatory mediators that amplify neuroinflammation. One of the primary triggers of NF-κB activation is the accumulation of amyloid-β (Aβ) aggregates. These toxic peptides stimulate NF-κB signaling in neurons and microglia, initiating inflammatory responses that impair synaptic function, promote neuronal death, and accelerate cognitive decline. NF-κB also plays a central role in controlling the expression and release of major pro-inflammatory cytokines such as TNF-, IL-6, and IL-1β. These cytokines can

reactivate NF-κB through both self-targeted (autocrine) and nearby cell-targeted (paracrine) pathways, forming a self-amplifying loop of inflammation that worsens neuronal damage and Alzheimer's disease (AD) progression [78]. Another important function of NF-κB is its role in turning on the NLRP3 inflammasome, a key part of the brain's immune defense. Aβ fibrils can trigger this inflammasome, and NF-κB boosts the production of NLRP3 needed for its formation. Once active, this leads to the release of inflammatory cytokines like IL-1β and IL-18. Studies in AD mouse models lacking NLRP3 or caspase-1 show better memory performance and faster Aβ clearance, pointing to the vital role of the NF-κB–NLRP3 pathway in AD development. Besides Aβ-related issues, NF-κB also affects the buildup and spread of tau proteins, another hallmark of AD. When activated in microglia, NF-κB increases the processing and release of tau clumps, which may trigger tau buildup in other brain areas. Interestingly, blocking NF-κB in models of tauopathy has led to reduced tau spread, highlighting its strong regulatory effect on tau pathology [77].

Moreover, NF-κB impacts AD pathology through modulation of specific microRNAs (miRNAs). Once activated, it upregulates several disease-associated miRNAs, including miR-9, miR-30b, miR-34a, miR-125b, miR-146a, and miR-155. These miRNAs contribute to various pathological features of AD, such as impaired clearance of Aβ, increased amyloidogenesis, astrogliosis, reduced neurotrophic support, neuronal atrophy, and disruptions in cytoskeletal and synaptic elements. Additionally, genetic factors also influence NF-κB activity in the context of AD. The APOE4 allele, a major genetic risk factor, is associated with heightened astrocyte-mediated inflammation and elevated expression of IL-6 and IL-8, potentially due to inadequate NF-κB repression. Mutations in upstream regulators of NF-κB, such as ADAM17 and SHARPIN, have also been implicated in AD, suggesting that dysregulation in this signaling pathway significantly contributes to disease susceptibility and progression [18, 78].

In the end, NF-κB-driven neuroinflammatory responses play a key role in causing synaptic dysfunction, nerve cell damage, and memory loss. When glial cells stay

activated for a long time, they continuously release harmful substances—mostly under the control of NF-κB—which gradually damage and destroy neurons.

2.12.4 Existing Therapies for Alzheimer's Disease

The current therapeutic strategies for Alzheimer's disease (AD) are primarily aimed at symptom management, with a growing focus on disease-modifying approaches. However, a definitive cure remains out of reach. Historically, treatment has centered on FDA-approved medications that offer temporary relief, particularly during the early to moderate stages of the disease. Among these, cholinesterase inhibitors—including donepezil, rivastigmine, and galantamine function by inhibiting the enzymatic breakdown of acetylcholine, a neurotransmitter essential for learning and memory. While initially beneficial, the effectiveness of these drugs tends to decline as the disease progresses and acetylcholine production diminishes. For individuals in moderate to severe stages of AD, memantine, an N-methyl-D-aspartate (NMDA) receptor antagonist, is commonly prescribed. It works by modulating glutamate activity, thereby protecting neurons from excitotoxic damage and supporting functional ability [79].

In recent years, considerable progress has been made with the introduction of anti-amyloid immunotherapies, marking a shift toward disease-modifying treatments (DMTs). Lecanemab, which received FDA approval, targets soluble β-amyloid aggregates, facilitating the reduction of amyloid plaque burden. Clinical trials have shown that Lecanemab slows cognitive decline in patients with early-stage AD over an 18-month period. Similarly, Aducanumab has been granted accelerated approval for use in early-stage AD, while Donanemab, approved in July 2024, has demonstrated potential in slowing both cognitive and functional deterioration during early symptomatic stages of the disease. Despite these advancements, the clinical benefits of anti-amyloid therapies remain modest, and many patients continue to experience disease progression. This underscores the multifactorial nature of AD, where amyloid accumulation is only one aspect of a complex pathological landscape. In particular, neuroinflammation has emerged as a key contributor to

disease progression, emphasizing the need for novel therapeutic approaches that go beyond amyloid targeting and address the broader mechanisms underlying AD pathology [80, 81].

Given the pivotal role of NF-κB in mediating neuroinflammation in Alzheimer's disease (AD), targeting this pathway represents a compelling therapeutic strategy to mitigate the chronic inflammatory responses that contribute to neuronal injury and disease progression [78]. Ongoing research is focused on developing selective NF-κB inhibitors that can modulate the pathway with minimal off-target effects, thus enhancing safety and therapeutic specificity. Several innovative approaches are currently under investigation. Mesenchymal stem cells (MSCs) and the retinoid drug acitretin have shown promise in regulating the NF-κB pathway by modulating inflammation-related microRNAs, such as miR-146a and miR-155, which are often dysregulated in AD. These interventions have demonstrated potential to restore normal inflammatory gene expression in animal models of AD [82]. Furthermore, a recombinant monomer of nuclear receptor-related protein 1 (Nurr1) has been identified to interact with the NF-κB p65 subunit, thereby suppressing the transcription of pro-inflammatory genes and reducing neuroinflammation in preclinical AD models [83]. Another notable candidate, Netrin-1 (NTN-1), has exhibited the ability to alleviate amyloid-β-induced microglial activation and memory deficits, likely through inhibition of both the NF-κB signaling cascade and the NLRP3 inflammasome [83]. Traditional therapeutic systems also offer potential. For instance, Qi Fu Yin (QFY), a formulation from Traditional Chinese Medicine, has shown anti-inflammatory effects in AD model rats by modulating the TLR4 and RAGE/NF-κB signaling pathways and reducing microglial overactivation [77, 84]. Similarly, nicardipine, a calcium channel blocker, has demonstrated neuroprotective effects by downregulating NF-κB activation and inhibiting interleukin-1β (IL-1β) release in Aβ-stimulated microglial cells [15]. Additionally, biologic agents such as etanercept, a TNF receptor 2 (TNFR2) fusion protein, have shown encouraging outcomes in early-stage studies. Etanercept appears to reduce NF-κB activation in glial cells by neutralizing TNF, suggesting a novel approach to modulate inflammatory responses in AD pathology [78].

2.13 Challenges in Developing NF-κB Modulators

While targeting the NF-κB pathway offers strong therapeutic potential in Alzheimer's disease (AD), developing effective and safe inhibitors remains a significant challenge. This is primarily because NF-κB plays a central role in many essential biological functions, especially in regulating immune responses, cell survival, and inflammation [82]. Direct inhibition of this pathway could lead to undesirable side effects, including the suppression of the normal immune system, which is vital for fighting infections and maintaining homeostasis. As a result, it is crucial to carefully balance the suppression of harmful inflammation with the preservation of necessary immune functions, to avoid unintended harm. Additionally, the exact role of NF-κB in AD pathogenesis is still being investigated. Researchers are working to identify which specific NF-κB subunits are most relevant in AD, and how glial cells and neurons interact through this pathway under disease conditions. A clearer understanding of the target genes regulated by NF-κB in both healthy and AD-affected brain cells is still needed [81]. Due to this complexity, the development of highly selective NF-κB inhibitors is essential. Such targeted therapies would ideally suppress only the disease-related actions of NF-κB while leaving its normal functions intact, ensuring both safety and therapeutic effectiveness.

2.14 Approaches in Synthetic Organic Chemistry

Organic synthesis plays a key role in scientific research and has had a strong impact on modern society. Over time, continuous technological progress and new discoveries have greatly improved the way chemists design and create new molecules [85]. In the 20th century, major developments in chemical synthesis led to the production of a wide variety of complex and diverse compounds. Although it is a well-established field, organic synthesis is still often seen as a mix of science

and creativity because new substances can sometimes be discovered unexpectedly. Today, there is increasing interest in creating molecules that perform specific and precise biological tasks. This has led to the development of stereoselective synthesis techniques, which help chemists produce molecules in exact forms, even in small amounts.

These carefully designed compounds are important not only for studying biological systems but also for developing new drug candidates. In particular, specialized resins and reactive intermediates are now widely used in both research and early drug discovery efforts [86].

2.15 Isolation and Purification Techniques in Synthesis

In organic synthesis, isolating and purifying the final product are essential steps after the reaction is complete. One commonly used method to monitor reaction progress and check product formation is Thin Layer Chromatography (TLC). It is a quick and simple technique that helps identify when the desired product has formed.

In some recent studies, TLC has been successfully combined with mass spectrometry (TLC-MS) to detect specific compounds from a synthetic mixture with greater accuracy [87].

After identifying the product, liquid-liquid extraction is often used to separate it from other substances in the reaction mixture. This method works by using solvents with different polarities, allowing the product to move into one layer while unwanted components stay in another. Solvent choices depend on the chemical nature of the product. Common solvents used include methanol, n-hexane, ethyl acetate, and chloroform, mixed in various ratios based on the product's solubility and polarity [88].

2.16 Chemical Characterization Techniques

2.16.1 FT-IR Spectroscopy

Fourier-Transform Infrared (FTIR) spectroscopy is a widely used technique in drug research for identifying functional groups and confirming the chemical structure of synthesized compounds. It works by measuring how a compound absorbs infrared light, producing a unique spectral fingerprint for each molecule. This fingerprint helps researchers confirm the identity of the compound and detect the presence of key functional groups. FTIR is also valuable for checking the purity and consistency of drug formulations. It can reveal if any contaminants are present or if unwanted chemical changes have occurred during synthesis or storage. Additionally, comparing FTIR spectra before and after a chemical modification allows researchers to verify whether the intended changes in the molecule have been successfully achieved. This makes FTIR an essential tool for both quality control and structural confirmation in pharmaceutical development [89, 90].

2.16.2 NMR Spectroscopy

Nuclear Magnetic Resonance (NMR) spectroscopy is a powerful and reliable tool used to study the structure and behavior of chemical compounds. It works by measuring the magnetic properties of certain atomic nuclei, especially those like hydrogen (^{1}H), carbon (^{13}C), and nitrogen (^{15}N), which naturally spin [91]. When these nuclei are placed in a strong magnetic field and exposed to radiofrequency (RF) waves, they absorb energy and switch between spin states. The resulting signal provides precise information about the chemical environment around each nucleus. NMR is widely used in pharmaceutical and biomedical research. It helps scientists understand how atoms are arranged in a molecule, the three-dimensional shape, and whether different forms of the same molecule (such as isomers or tautomers) are present. This is especially important in drug discovery, where the correct shape and form of a molecule can affect how well it works [92]. NMR also plays a key role in structural biology, helping to explore how drugs interact

with their targets like proteins or DNA. Because it gives clear, detailed, and non-destructive data, NMR remains one of the most important techniques for analyzing drug compounds [93, 94].

2.17 Integrating Computational and Experimental Drug Discovery

Modern drug discovery has greatly advanced by combining experimental techniques like FTIR, NMR, and organic synthesis with powerful computational tools. These computer-based methods include pharmacophore modeling, molecular docking, computer-aided drug design (CADD), molecular dynamics (MD) simulations, and in-silico ADMET profiling. Together, they provide a detailed understanding of how drug molecules interact with their targets. Pharmacophore modeling helps identify the key chemical features that a molecule must have to show biological activity. CADD uses smart algorithms to design and improve chemical structures for better interaction with biological targets, making the drug discovery process faster and more efficient. Molecular docking shows how well a drug fits into its target site and helps predict its binding strength. MD simulations go further by showing how drug molecules and proteins move and change shape over time, giving a realistic picture of their interaction inside the body [95, 96]. In-silico ADMET analysis predicts how a drug will behave in the body—how it is absorbed, distributed, metabolized, and removed, as well as any toxic effects it may cause. This helps select the best drug candidates early, saving time and reducing costs in lab testing [20]. When these computational methods are combined with laboratory-based techniques like NMR and FTIR, researchers can validate their predictions with real-world data. This integrated approach provides a complete picture of how a drug works, which helps in designing better, safer, and more effective medicines. It also reduces unnecessary experiments and increases the chances of success in drug development [95].

Chapter 3

Materials and Methods

A schematic representation of the methodology followed in the present study is illustrated in Figure 3.1

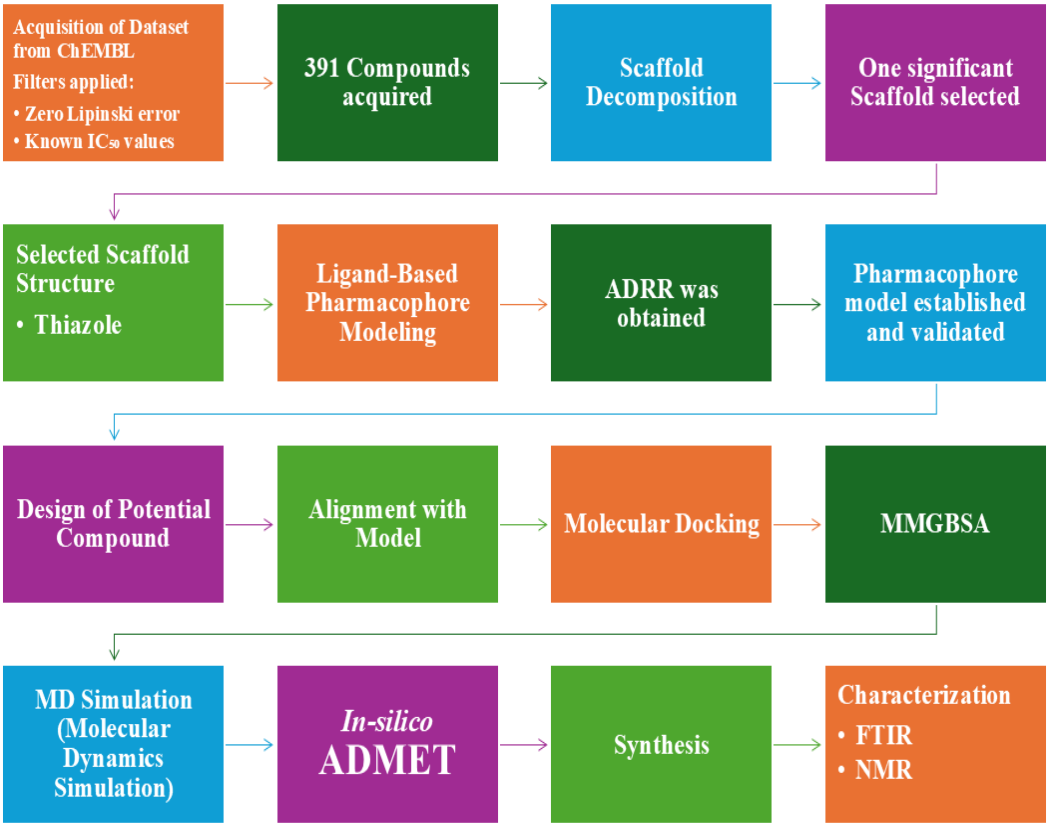

FIGURE 3.1: A stepwise diagram displaying the complete methodological framework adopted in this study, from computational modeling to experimental validation.

3.1 Part A: Pharmacophore Modeling, Drug Design and Computational Analysis

3.1.1 Data Collection and Curation

Pharmacophore modeling was initiated by compiling a dataset of established NF-κB inhibitors retrieved from the ChEMBL database. ChEMBL is an open-access platform that offers comprehensive information on bioactive molecules, including their chemical structures, pharmacological activities, target interactions, and ADMET characteristics, making it a valuable tool for drug discovery studies [8, 99]. In this study, the selected target protein was human NF-κB, identified as ChEMBL2094258 in the ChEMBL database and as P19838 in UniProt. A total of 393 NF-κB inhibitors with reported IC values were initially retrieved from ChEMBL. To refine the dataset and ensure its reliability, multiple filters were applied. Compounds that did not comply with Lipinski's Rule of Five were excluded, only single protein in-vitro assay data were considered, and molecules with known pChEMBL values were selected. After applying these criteria, a set of 316 high-confidence inhibitors was finalized. These compounds were arranged in a tab-separated values (TSV) file that included key properties such as molecular weight, pChEMBL value, ALogP (lipophilicity), IC (in nM), and SMILES (Simplified Molecular Input Line Entry System) strings. The SMILES representations were then converted into 3D SDF (Structure Data File) format using the Online SMILES Translator by the NCI/CADD Group (https://cactus.nci.nih.gov/translate/), and these 3D structures were used for downstream molecular modeling and pharmacophore development [100].

3.1.2 Identification of Molecular Scaffold

To better understand the core structures of the selected compounds, the refined dataset of 316 NF-κB inhibitors was analyzed for scaffold classification using the Schrödinger Maestro Suite [97]. Scaffold decomposition is a process that groups

compounds into different classes based on their core structures, mainly focusing on the number of rings or ring systems present in each molecule [98, 99]. This analysis revealed a wide range of structurally diverse scaffolds. These scaffolds were sorted and organized according to the number of ring systems they contained. After a thorough review of all the scaffold groups, the Thiazole scaffold was specifically selected for further study due to its recurring presence and potential relevance in NF-κB inhibition. This scaffold was then taken forward for more detailed analysis and pharmacophore modeling. Figure 3.1 shows the chemical structure of the acquired and chosen scaffold.

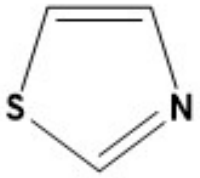

Thiazole

FIGURE 3.2: The chosen scaffold for the subsequent pharmacophore modeling

3.1.3 Dataset Division for Model Development

After selecting the Thiazole scaffold, a total of 92 molecules containing this core structure were extracted for pharmacophore model development. To build and validate the model properly, these molecules were divided into training and test sets using a random split ratio of 70:30. As a result, 65 compounds were assigned to the training set, while 27 compounds were included in the test set. To ensure that the molecules were in their biologically relevant forms, both sets were processed using LigPrep [100] and EPIK [101]. These tools were used to generate the most likely tautomeric and protonation states of the molecules at physiological pH (7.0 $\pm$ 2). Following this, each compound was subjected to energy minimization using the OPLS4 force field under default settings, helping to optimize their geometry for better accuracy in further modeling [102].

Next, multiple conformers were generated for each molecule using the "Create Phase Database" wizard in the Schrödinger Suite. This step was essential to increase the structural diversity of the compounds, which is important for identifying the most likely bioactive conformations during pharmacophore modeling. This comprehensive preparation ensured that all compounds were properly optimized for accurate and reliable pharmacophore generation and validation [13].

3.1.4 Generation of Pharmacophore Hypotheses

To identify the key structural features responsible for binding with the target protein NF-κB, pharmacophore models were generated using the PHASE module from the Schrödinger Suite [103, 104]. A ligand-based approach was applied to the previously prepared training set, aiming to uncover the essential chemical features required for biological activity [103].

Compounds were classified as either active or inactive based on their pChEMBL values. Specifically, molecules with pChEMBL values greater than 5.6 were labeled as active, while those with values below 5.6 were considered inactive. This threshold was used to guide the generation of pharmacophore hypotheses from the most biologically relevant compounds. The pharmacophore features were defined using six key elements provided by the PHASE software i.e. Hydrogen bond acceptor (A), Hydrogen bond donor (D), Aromatic ring (R), Hydrophobic group (H), Negatively ionizable (N) and Positively ionizable (P).

To improve the accuracy of the model, excluded volume shells were enabled for both active and inactive molecules. These shells help to highlight regions in space that are unfavorable for ligand binding. Each pharmacophore hypothesis was designed to include 4 to 5 features, and some restrictions regarding the minimum number of features were disabled to allow broader model exploration and increased flexibility in hypothesis generation. This strategic approach ensured that a wide range of pharmacophore hypotheses were explored, enhancing the chances of identifying a robust and predictive model.

3.1.5 Validation of Pharmacophore Model

The performance of the generated pharmacophore model(s) was evaluated using a test set of 27 compounds. This validation step aimed at assessing the model's ability to accurately identify active compounds from a pool of molecules. To strengthen this evaluation, a decoy set was created using the DUD.E (Database of Useful Decoys: Enhanced) [105], The SMILES strings of the test set compounds were used as input for decoy generation, resulting in 1,100 structurally similar but presumed inactive molecules. This combined dataset of actives (test set) and decoys provided a robust platform to thoroughly assess the discriminative power of the pharmacophore model.

The PHASE module's Enrichment Viewer Wizard was used to analyze the performance. A detailed review of the enrichment reports was conducted for each pharmacophore model. These reports offered key insights into how effectively the model could distinguish between active compounds and decoys. Metrics such as early enrichment, ROC curves, and goodness-of-hit scores were examined to determine the predictive accuracy and screening efficiency of the models.

3.1.6 Design Strategy for Novel Inhibitor(s)

Potential inhibitors were designed using a structure-based drug design (SBDD) approach. These molecules were specifically developed to align closely with the validated pharmacophore model, ensuring that they matched as many pharmacophoric features as possible. By incorporating key interaction points identified in the pharmacophore—such as hydrogen bond donors/acceptors, hydrophobic groups, and aromatic rings—the designed compounds were optimized to enhance their binding potential with the NF-κB active site. This rational design strategy aimed to produce novel inhibitor structures with strong predicted affinity and favorable interaction profiles.

3.1.7 Molecular Docking Studies

For this study, the high-resolution X-ray crystal structure of the human NF-κB protein (PDB ID: 7VUP; resolution: 2.70 Å) was obtained from the Protein Data Bank [110, 111]. The structure was prepared using the Protein Preparation Wizard in the Schrödinger Suite, which involved preprocessing, assigning bond orders, adding hydrogen atoms, optimizing hydrogen bonding networks, and performing restrained energy minimization [106]. uring the receptor grid generation step, a docking grid was defined around the protein's active binding site using Cartesian coordinates (x = 10.5, y = 70.6, z = 22.68). A scaling factor of 1.0 Å was applied to the van der Waals radii of receptor atoms to allow flexibility and improve docking accuracy.

Molecular docking was carried out using the Glide module in Extra Precision (XP) mode to ensure more reliable and accurate predictions of ligand binding poses and interaction profiles [113]. This high-precision docking protocol allowed for the detailed evaluation of how designed and screened ligands interact with the NF-κB binding site, supporting the identification of potential inhibitors [107].

3.1.8 MM-GBSA Bond Energies

To gain deeper insights into the binding strength and the impact of solvent on ligand–protein interactions, MM-GBSA (Molecular Mechanics–Generalized Born Surface Area) calculations were conducted using the PRIME module of the Schrödinger Suite. This computational approach estimates the binding free energy of ligands by accounting for both molecular mechanics and solvation contributions, offering a more realistic evaluation of binding affinity [108, 109].

The analysis was conducted on XP-docked complexes, utilizing Pose Viewer files generated during the docking process. Prior to the MM-GBSA calculations, each complex was energy-minimized using PRIME's local optimization tool to enhance stability and precision. The calculations employed the OPLS4 force field for evaluating molecular interactions [110], while rotamer search algorithms were used to

optimize the side-chain conformations of amino acid residues within the binding site [111].

The VSGB solvation model was applied to simulate the aqueous environment and better represent solvent effects [112]. This MM-GBSA approach enabled a comprehensive analysis of binding energetics by incorporating both non-bonded interaction energy and solvation contributions, offering deeper insight into the thermodynamic favorability of ligand binding to the NF-κB protein.

3.1.9 Molecular Dynamic Simulations

To gain deeper insight into the dynamic stability and conformational behavior of the most promising ligand–NF-κB complex (selected based on its lowest MM-GBSA binding free energy), molecular dynamics (MD) simulations were conducted using the DESMOND module within the Schrödinger Suite [42].

Initially, the system was built using the System Builder panel, where an orthorhombic simulation box was defined with a 10 Å buffer region around the protein to avoid periodic boundary artifacts. The system was solvated using an explicit TIP3P water model, and 150 mM NaCl was added to neutralize the system and simulate physiological ionic strength.

To minimize steric clashes and stabilize the system before the production run, 2000 iterations of energy minimization were performed. The production MD simulation was executed for a total of 200 nanoseconds (ns) under NPT (constant pressure and temperature) ensemble conditions. The temperature was maintained at 300 K using the Nose–Hoover Chain thermostat [120] and the pressure was kept at 1.01 bar using the Martyna–Tobias–Klein barostat [113]. The simulation was carried out with a 2 nanosecond (ns) time step. Throughout the simulation, trajectory snapshots capturing energy, atomic positions, and conformational changes were recorded at 10 picosecond (ps) intervals. Post-simulation, the MAESTRO interface was employed to analyze structural fluctuations, protein–ligand interactions, and binding stability over time.

3.1.10 Prediction of ADMET Properties

The selected potential NF-κB inhibitor was subjected to in-silico ADMET (Absorption, Distribution, Metabolism, Excretion, and Toxicity) profiling using ADMET Predictor® 12.0, a robust and industry-standard computational platform hosted on the Simulation Plus Cloud Server (64-bit edition).

All evaluations were performed under physiological pH conditions (7.4) to simulate human biological environments. A comprehensive set of pharmacokinetic and toxicity-related parameters was predicted to assess the molecule's drug-likeness, including properties related to intestinal absorption, blood–brain barrier permeability, cytochrome P450 metabolism, renal clearance, and hepatotoxicity.

This predictive profiling provided essential insights into the compound's pharmacological behavior, bioavailability, and safety profile, thereby aiding in the early-stage selection of viable drug candidates for further experimental validation.

3.2 Part 2: Synthesis and Characterization of Potential inhibitor(s)

3.2.1 Chemicals

The chemicals required for the current study include Ketorolac (255.27 g/mol), Diclofenac acid (296.15 g/mol), Para-Nitroaniline (138.13 g/mol), Anisidine (123.15 g/mol) and Para-Toluidine (107.15 g/mol) sourced from Nimral Pharmaceutical Pvt. Ltd., and several reagents from Sigma Aldrich such as Triethylamine (101.19 g/mol), Thionyl Chloride (118.97 g/mol), Potassium Carbonate (138.21 g/mol), Doxorubicin (543.52 g/mol) and DMAP (122.17 g/mol). Additionally, p-Nitro Aniline with a molar mass of 138.13 g/mol was procured from Macklin. All used analytical-grade solvents were sourced from Sigma-Aldrich Private Limited, a leading supplier of laboratory chemicals.

3.2.2 Solvents

The solvents used in the present study were all purchased from Sigma Aldrich, Germany. These include dichloromethane, ethyl acetate, acetonitrile, n-hexane, chloroform, petroleum ether, ethanol, and methanol.

3.2.3 Equipment

The equipment used in the present study included a TLC plate (Silica Gel 60 F254) from Merck Pharma, and a rotary evaporator (RE 200) from Bibby Starlin Ltd, England. Additional instruments used were a magnetic stirrer/hot plate (MS-H280-Pro) from Merck Pharma, Microplate Reader HF4500 from Meizheng Bio-Tech Company, FTIR spectrometer (Cary630) from Agilent Analytical Technologies, and a pH meter (PHS, 25GW) from Banta Instruments, USA.

3.2.4 Synthesis of Potential Inhibitor

3.2.4.1 Synthesis of MAS-1

The synthesis of the target compound, MAS-1, was performed through a two-step reaction process. Initially, 10 mL of dichloromethane (DCM) was added to a clean round-bottom flask. To this, 300 mg (0.1 mmol) of ketorolac and 0.98 mL (0.1 mmol) of triethylamine were introduced. The reaction mixture was cooled using an ice bath and stirred for 15 minutes to maintain a stable temperature. Following this, 0.1 mL (0.1 mmol) of thionyl chloride was carefully added dropwise through a dropping funnel while keeping the reaction on ice. Stirring was continued under cold conditions for 30 minutes, and the reaction progress was monitored by thin-layer chromatography (TLC) using an ethyl acetate:n-hexane (1:2) solvent system. After confirming initial conversion, the reaction was allowed to reach room temperature and was further stirred for 2 hours. It was then refluxed at 60°C for 1 hour to ensure completion. The solvent was removed under reduced pressure using

a rotary evaporator, yielding a brownish-black crude intermediate. This intermediate was weighed (excluding the glassware) and directly used for the next step without further purification. In the second step, 12.3 mg (0.1 mmol) of p-anisidine and 144 mg (0.5 equivalents) of DMAP were dissolved in 10 mL of DCM to prepare a fresh solution. This solution was added to the previously obtained crude product. The resulting mixture was stirred overnight at room temperature, and the reaction progress was monitored periodically using the same TLC conditions. Upon completion, the solvent was evaporated under reduced pressure. The residue was then treated with acetone, and the pH was adjusted to neutral using a saturated potassium chloride (KCl) solution to remove any unreacted ketorolac. To precipitate the final product, cold distilled water was added dropwise. The solid formed was collected through vacuum filtration, washed thoroughly with acetone, and left to dry at room temperature. The final compound, MAS-1, was obtained as a black-colored solid [114, 115].

3.2.4.2 Synthesis of MAS-2

In the first step, 10 mL of dichloromethane (DCM) was added to a clean round-bottom flask. Then, diclofenac acid (29.6 mg, 0.1 mmol) and triethylamine (0.98 mL, 0.1 mmol) were added. The reaction flask was placed in an ice bath and stirred for 15 minutes to activate the reaction environment. After this, thionyl chloride (0.1 mL), equimolar to diclofenac acid, was slowly added using a dropping funnel while keeping the temperature low. Stirring continued under cold conditions for 30 minutes. The progress of the reaction was checked by thin-layer chromatography (TLC) using a solvent system of ethyl acetate and n-hexane (1:2). The reaction mixture was then allowed to reach room temperature and stirred for an additional 2 hours. To ensure full conversion, the mixture was refluxed at 60°C for 1 hour. The solvent was then evaporated under reduced pressure using a rotary evaporator. A brownish-black crude intermediate was obtained, which was dried and weighed (glassware weight excluded).

In the second step, p-toluidine (10.7 mg, 0.1 mmol) was dissolved in 10 mL of DCM. To this solution, 0.5 equivalents of DMAP (6.1 mg, MW 122.17 g/mol) were added

as a catalyst. This freshly prepared solution was then added to the intermediate obtained from the first step. The combined mixture was stirred overnight at room temperature. The reaction progress was again monitored by TLC using the same solvent system. After completion, the solvent was removed under reduced pressure. The remaining residue was transferred to a beaker containing acetone. The pH was adjusted to neutral using concentrated potassium chloride (KCl) solution to remove any unreacted diclofenac acid. To isolate the final product, cold distilled water was added dropwise to the reaction mixture. The resulting solid was collected by vacuum filtration, thoroughly washed with acetone, and dried at room temperature. The final compound, named MAS-2, was obtained as a reddish-brown solid [114, 115].

3.2.4.3 Synthesis of MAS-3

In the initial stage of synthesis, 10 mL of dichloromethane (DCM) was poured into a clean round-bottom flask. Ketorolac (300 mg, 0.1 mmol) and triethylamine (0.98 mL, 0.1 mmol) were then added. The mixture was placed in an ice bath and stirred gently for 15 minutes to allow thorough mixing under low-temperature conditions. Following this, thionyl chloride (0.1 mL, equimolar to ketorolac) was added slowly using a dropping funnel while maintaining the chilled environment. The reaction was continued on ice for 30 minutes, and its progress was tracked through thin-layer chromatography (TLC), using an ethyl acetate and n-hexane mixture (1:2) as the mobile phase. The reaction mixture was then brought to room temperature and stirred for an additional 2 hours. To ensure complete activation, the contents were refluxed at 60°C for one hour. Afterward, the solvent was removed under reduced pressure using a rotary evaporator. The resulting brownish-black crude intermediate was collected, dried, and weighed (excluding glassware weight) for use in the subsequent step.

In the second phase, p-nitroaniline (162.2 mg, 0.1 mmol) was dissolved in 10 mL of DCM, and 144 mg (0.5 equivalents) of DMAP was added as a catalyst. This solution was added to the previously obtained intermediate. The mixture was stirred at room temperature overnight, and TLC was again used to monitor the

progress under the same solvent system. After completion, the reaction mixture was concentrated under reduced pressure. The residue was transferred to a beaker using acetone, and the pH was adjusted using concentrated potassium chloride (KCl) solution to remove any unreacted ketorolac. Cold distilled water was added dropwise to facilitate precipitation of the final product. The solid was collected by vacuum filtration, washed thoroughly with acetone, and dried at room temperature. The final product, named MAS-3, was obtained as a violet-black crystalline solid [114, 116].

3.2.5 Characterization of synthesized compounds

3.2.5.1 Fourier Transform Infra-red

Fourier-transform infrared (FTIR) spectroscopy was performed for all synthesized compounds using a Cary 630 FTIR spectrometer (Agilent Technologies) in transmittance mode. The spectra were recorded at a resolution of 1 cm^{1}, covering the wavenumber range from 4000 to 650 cm^{1}. All measurements were conducted at a constant room temperature of 25°C. This analytical method was used to identify the functional groups present and to confirm the structural characteristics of the synthesized compounds.

3.2.5.2 Nuclear Magnetic Resonance

Nuclear Magnetic Resonance (NMR) served as a key analytical tool for determining molecular structures, as well as for quality control and research to evaluate the composition and purity of samples.

This technique was based on the interaction between magnetic fields and the magnetic moments of atomic nuclei. The magnetic moment of a nucleus arose from its angular momentum, which was generated by the nucleus spin. The magnitude of this spin was quantified by a value known as the spin number which was vital for understanding the nuclear spin behavior.

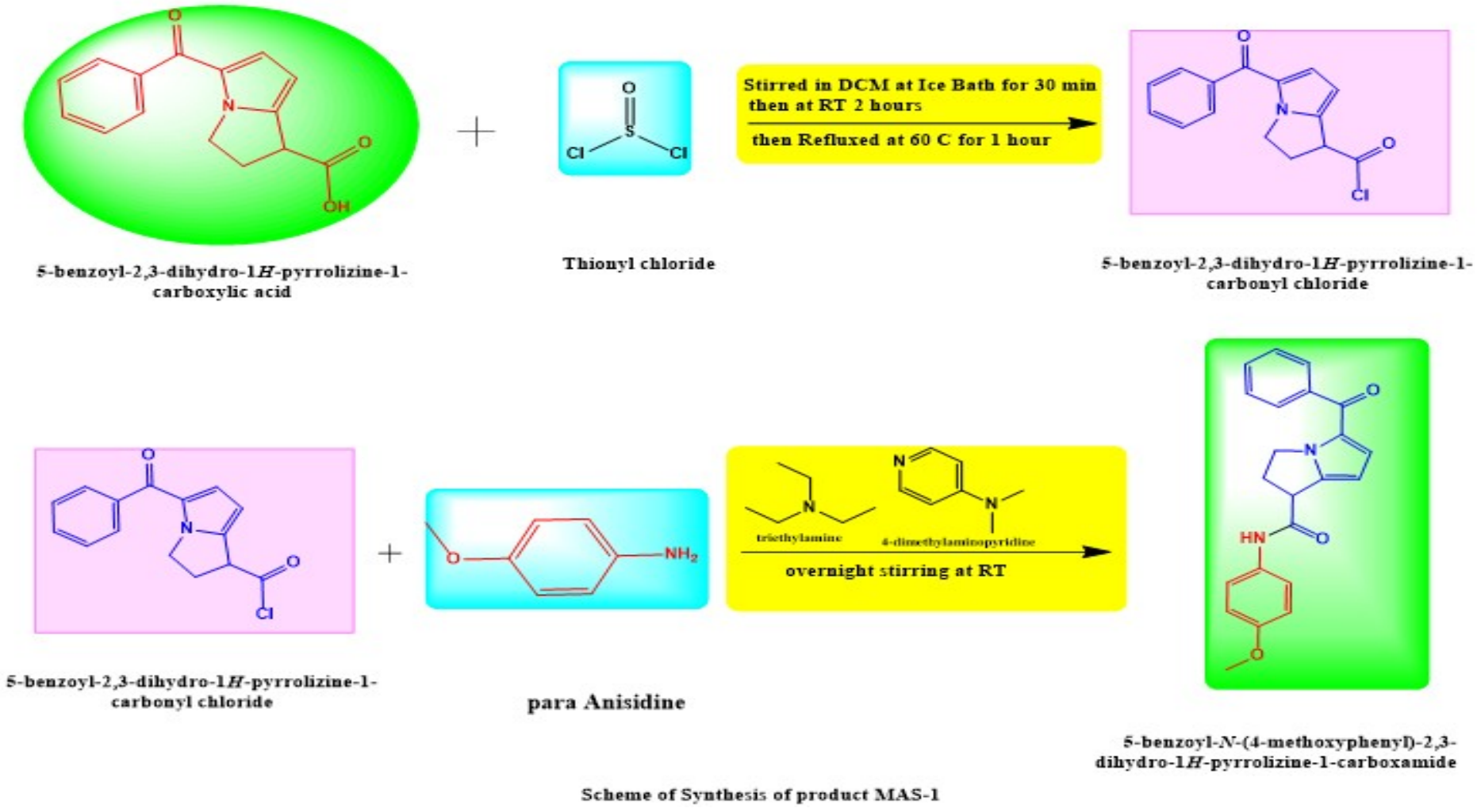

FIGURE 3.3: Scheme of synthesis of MAS-1

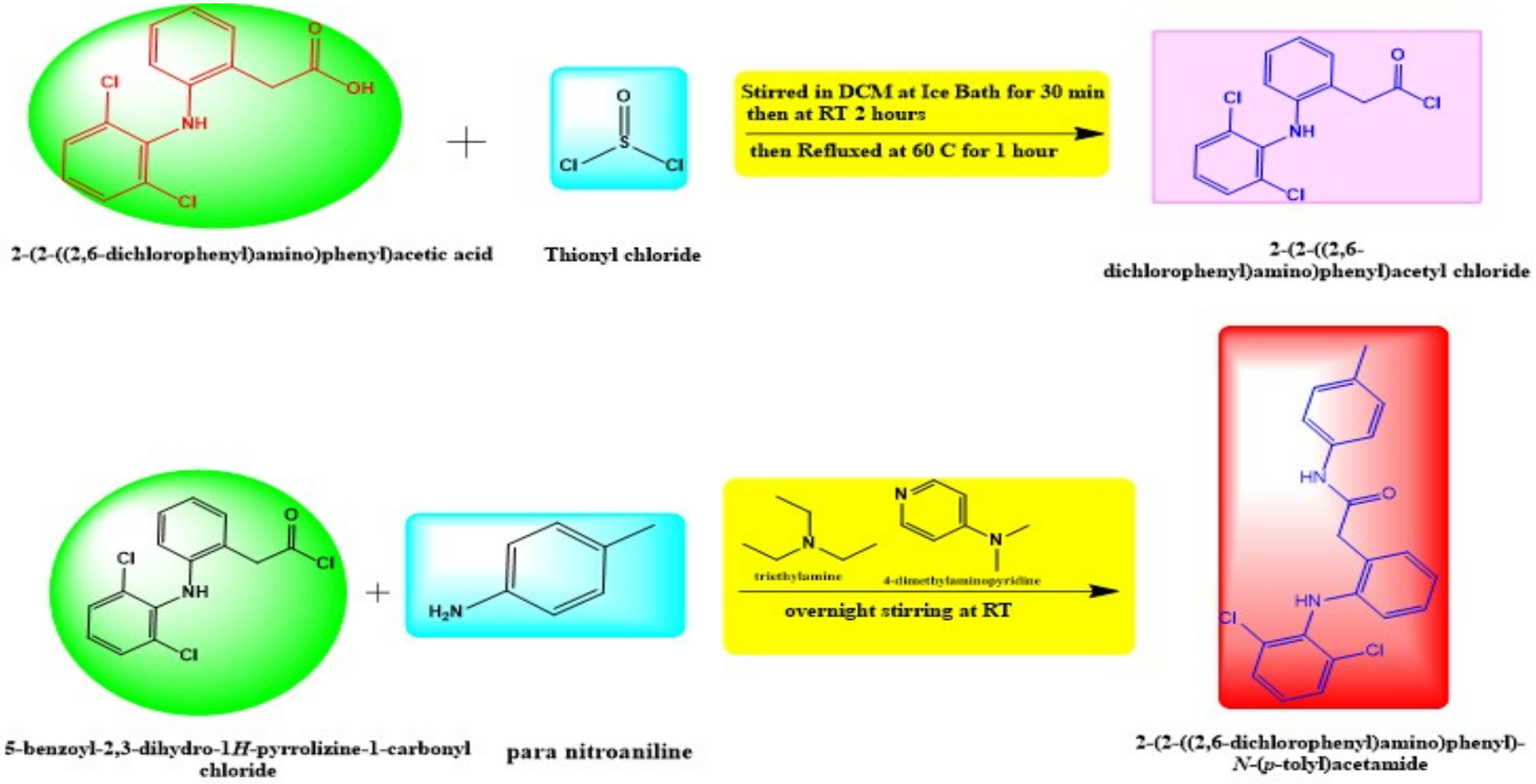

Scheme of Synthesis of product MAS-2

FIGURE 3.4: Scheme of synthesis of MAS-2

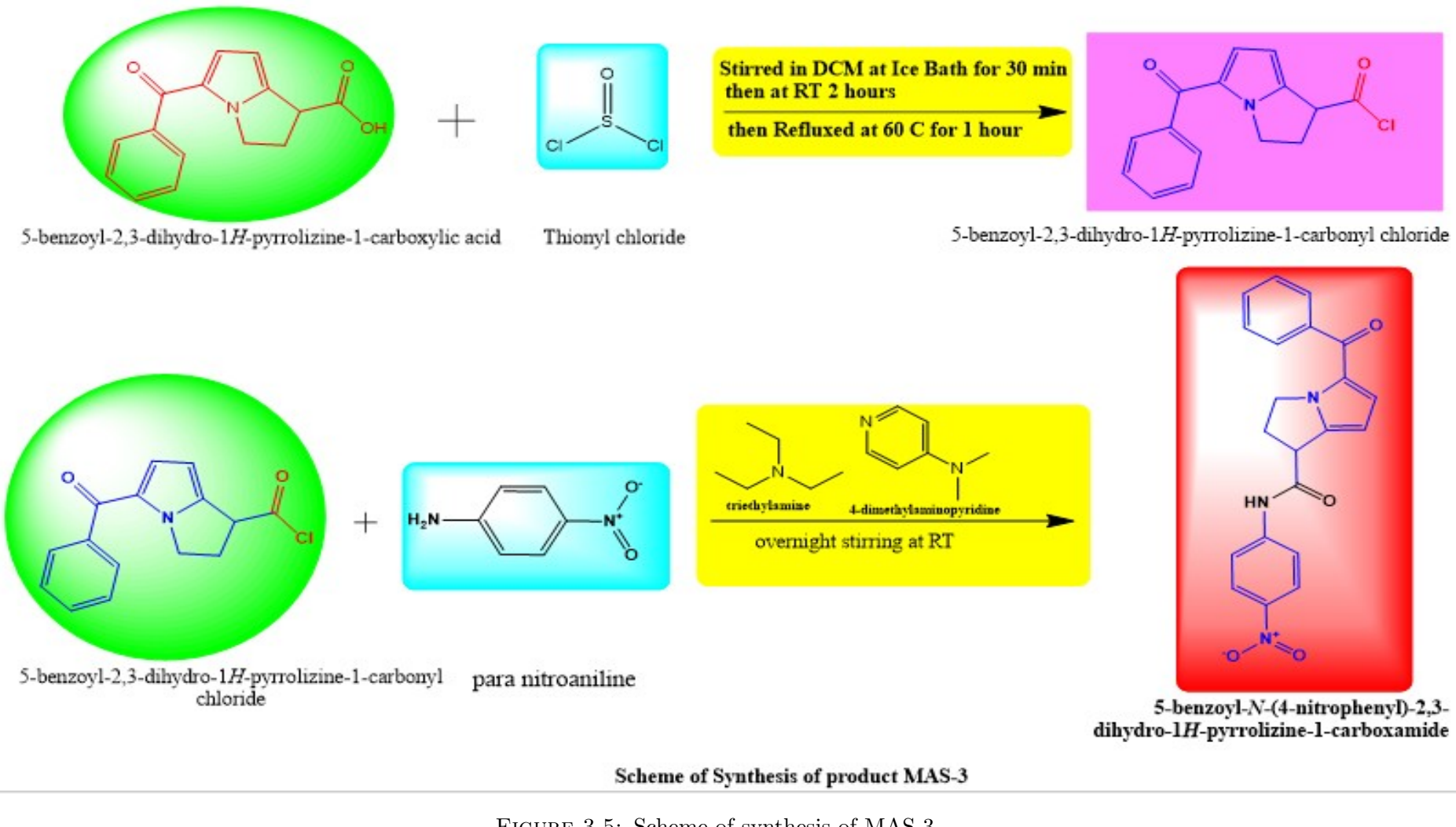

FIGURE 3.5: Scheme of synthesis of MAS-3

The properties of nuclear spin, including the spin number, were used to define the characteristics of the nucleus. In cases where a nucleus contained an equal number of protons and neutrons, both its nuclear spin and magnetic moment were effectively zero.

3.2.6 Biological Evaluation

3.2.6.1 Brine Shrimp Cytotoxicity Assay

Eggs from brine shrimp (*Artemia salina*) were used in this investigation and conventional protocols were followed, as described elsewhere [117]. To promote larval emergence, the eggs were incubated in simulated sea water for 24 to 48 hours. After reaching maturity, nauplii were removed from the hatching environment and a particular quantity was placed into each well of a 96-well plate. 1, 0.5, 0.25 and 0.125 mg/ml final concentrations of synthesized compound in $\leq$1% DMSO were used. Wells containing only seawater and nauplii along with negative control (1% DMSO) and positive control (doxorubicin) were used as controls. The plate was incubated for 24 hours under regulated conditions at 34°C.

Counting the number of living shrimp in each well allowed for the assessment of post-incubation shrimp mortality. Next, the percentage of dead shrimp at each concentration were determined using this data. The experiment was conducted in triplicate, and statistical analysis was performed. Percentage inhibition was calculated using mean and standard deviation to determine the median lethal concentration of the compound [118].

3.2.6.2 Antioxidant Assay

The DPPH (2,2-diphenyl-1-picrylhydrazyl) assay is a widely used in vitro method to evaluate antioxidant activity by measuring the ability of compounds to scavenge free radicals. When antioxidants donate electrons or hydrogen atoms to the stable purple DPPH radical, it reduces to a yellow-colored compound, with the extent

of discoloration measured at 517 nm. This change helps determine the percentage of radical inhibition or IC values. Over the last five years, numerous studies have applied the DPPH assay to assess antioxidant potential in plant extracts, isolated phytochemicals, synthetic compounds, and nanoparticle formulations [119, 120]. The DPPH assay remains a fast, reliable screening tool, especially in early-stage drug discovery. In the context of Alzheimer's disease (AD), oxidative stress plays a crucial role in neuronal damage and cognitive decline. Compounds with strong DPPH radical scavenging properties may offer neuroprotective benefits, making this assay valuable in identifying potential anti-Alzheimer agents through their antioxidant effects [121, 122].

Chapter 4

Results and Discussion

4.1 Phase Database Preparation for Training Set Molecules

Initially, a training set containing 65 well-characterized NF-B inhibitors was selected, each having clearly defined IC and pChEMBL values. These compounds were used to create a Phase database that served as the foundation for the pharmacophore modeling process. During database generation, stereoisomers of each compound were produced carefully certain chiral centers were kept fixed to maintain structural accuracy, while flexibility was allowed in others to capture possible bioactive forms.

To ensure efficiency and reliability, the database was optimized to include only the most stable conformations. Specifically, for molecules containing 4- or 5-membered rings, only one low-energy stereo-conformation was retained, while up to four of the lowest-energy stereoisomers were preserved for the remaining compounds. This balanced strategy maintained both structural diversity and energetic stability, ensuring that the final Phase database represented a realistic and chemically meaningful set of conformers suitable for subsequent pharmacophore modeling and virtual screening.

4.2 Feature Analysis of Final Pharmacophore Model

Using the previously prepared Phase database and the selection criteria outlined in Chapter 3, a pharmacophore model was developed. Based on the defined threshold pChEMBL value of 5.8, a total of 39 compounds out of the 65 in the training set were classified as active. In contrast, the remaining 26 compounds, with pChEMBL values below the threshold, were labeled as inactive. The inactive compounds included molecules numbered: 1, 3, 4, 8, 12, 18, 19, 20, 22, 23, 24, 26, 31, 32, 35, 36, 40, 42, 43, 46, 53, 55, 57, 58, 59, 61, and 62. These exhibited IC values ranging from 2623 nM to 35,510 nM, specifically: 7971, 5531, 11109, 35510, 6164, 14114, 4542, 5813, 2623, 2977, 3441, 3230, 10182, 4685, 3855, 2774, 4163, 5974, 3700, 15636, 6999, 2661, 2636, 2663, and 2623 nM, respectively. All the compounds in training set along with their respective IC50 and pChEMBL values are shown Figure 4.1 (Figure 4.1 is spilt into 4 parts).

In the result of the pharmacophore modeling process, a 4-feature hypothesis labeled ADRR (comprising Aromatic ring, Hydrogen bond Donor, and two Hydrogen bond Acceptors) was successfully generated. This hypothesis demonstrated strong model quality as indicated by several key performance metrics.

Specifically, the model achieved a survival score of 5.036, a volume score of 0.721, a site score of 0.784, a vector score of 0.871, a BEDROC score of 0.628, and a PhaseHypoScore of 0.930. Each of these metrics (except PhaseHypoScore and survival score) has a maximum possible value of 1, where scores closer to 1 reflect higher model reliability.

The PhaseHypoScore, a specific measure of model performance, also suggests better accuracy when its value is high. The obtained values, particularly the high PhaseHypoScore and vector score, indicate that the ADRR hypothesis is a well-optimized and predictive pharmacophore model. These results, combined with a strong survival score, suggest

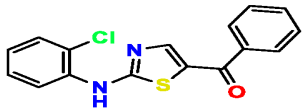

Compound #1
IC50 (nM): 7971
pChEMBL: 5.1

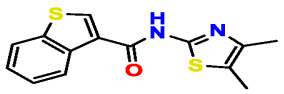

Compound #2
IC50 (nM): 943
pChEMBL: 6.03

Compound #3
IC50 (nM): 5531
pChEMBL: 5.26

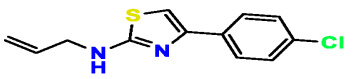

Compound #4
IC50 (nM): 11109
pChEMBL: 4.9

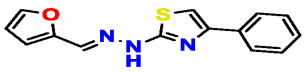

Compound #5
IC50 (nM): 1699
pChEMBL: 5.77

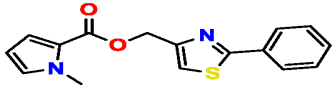

Compound #6
IC50 (nM): 768
pChEMBL: 6.12

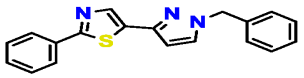

Compound #7
IC50 (nM): 2240
pChEMBL: 5.65

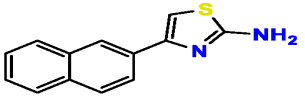

Compound #8
IC50 (nM): 35510
pChEMBL: 4.45

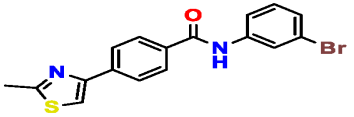

Compound #9
IC50 (nM): 1758
pChEMBL: 5.75

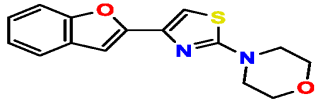

Compound #10
IC50 (nM): 966
pChEMBL: 6.01

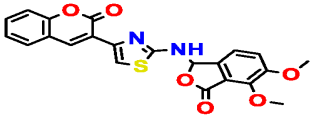

Compound #11
IC50 (nM): 2104
pChEMBL: 5.1

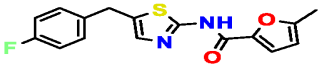

Compound #12
IC50 (nM): 6164
pChEMBL: 5.21

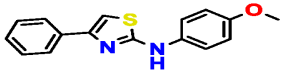

Compound #13
IC50 (nM): 752
pChEMBL: 6.12

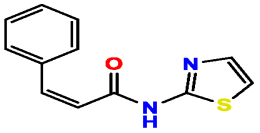

Compound #14
IC50 (nM): 1067
pChEMBL: 5.97

Compound #15
IC50 (nM): 2331
pChEMBL: 5.63

Compound #16
IC50 (nM): 1396
pChEMBL: 5.86

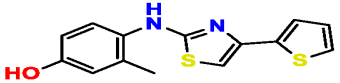

Compound #17
IC50 (nM): 1513
pChEMBL: 5.82

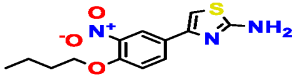

Compound #18
IC50 (nM): 14114
pChEMBL: 4.85

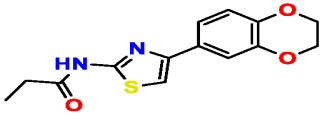

Compound #19
IC50 (nM): 4542
pChEMBL: 5.34

Compound # 20
IC50 (nM): 5813
pChEMBL: 5.24

Compound #21
IC50 (nM): 160
pChEMBL: 6.8

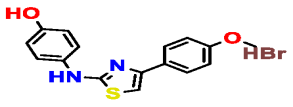

Compound #22
IC50 (nM): 2623
pChEMBL: 5.58

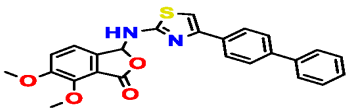

Compound #23
IC50 (nM): 2977
pChEMBL: 5.53

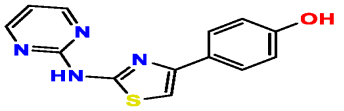

Compound #24
IC50 (nM): 3441
pChEMBL: 5.46

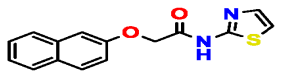

Compound #25
IC50 (nM): 776
pChEMBL: 6.11

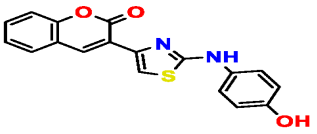

Compound #26
IC50 (nM): 3230
pChEMBL: 5.49

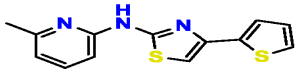

Compound #27
IC50 (nM): 1224
pChEMBL: 5.91

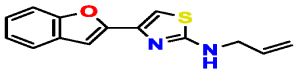

Compound #28
IC50 (nM): 598
pChEMBL: 6.22

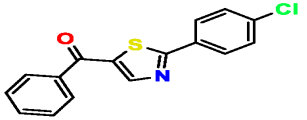

Compound #29
IC50 (nM): 1250
pChEMBL: 5.9

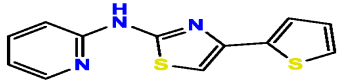

Compound #30
IC50 (nM): 667
pChEMBL: 6.18

Compound #31
IC50 (nM): 10182
pChEMBL: 4.99

Compound #32
IC50 (nM): 4685
pChEMBL: 5.33

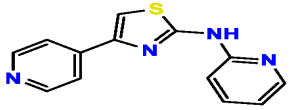

Compound #33
IC50 (nM): 1642
pChEMBL: 6.18

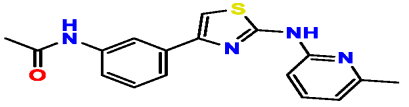

Compound #34
IC50 (nM): 1634
pChEMBL: 5.79

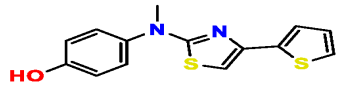

Compound #35
IC50 (nM): 3855
pChEMBL: 5.41

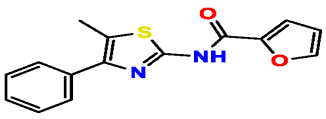

Compound #36
IC50 (nM): 2774
pChEMBL: 5.56

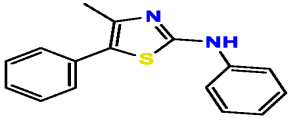

Compound #37
IC50 (nM): 1449
pChEMBL: 5.84

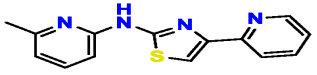

Compound #38
IC50 (nM): 1192
pChEMBL: 5.92

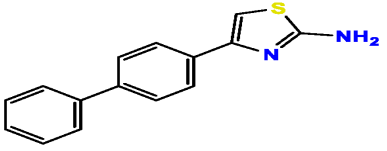

Compound #39
IC50 (nM): 2421
pChEMBL: 5.62

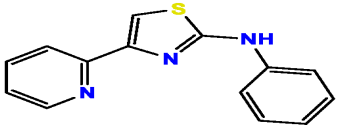

Compound #40
IC50 (nM): 4163
pChEMBL: 5.38

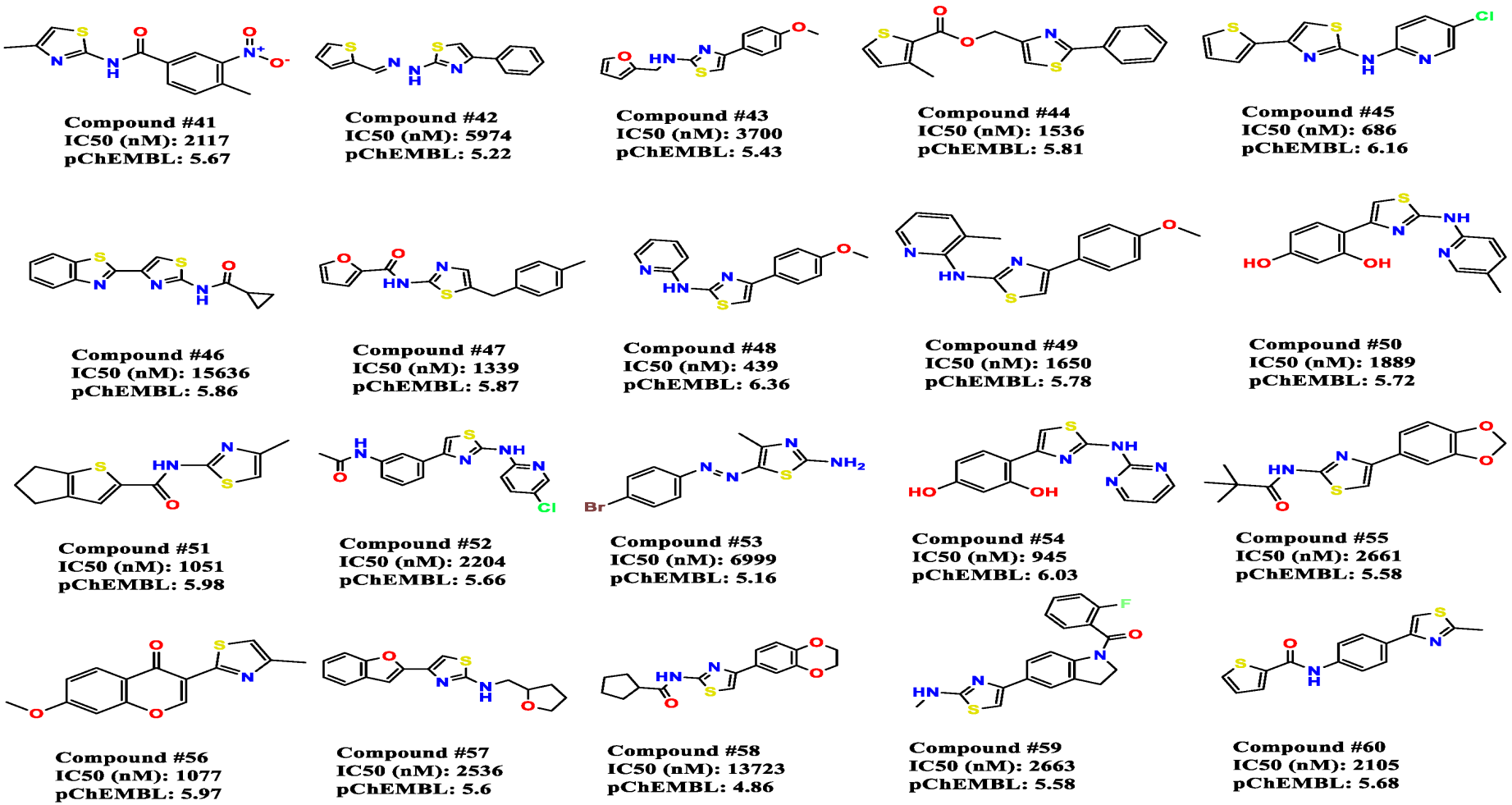

FIGURE 4.1: All 65 training set molecules with their corresponding IC50 and pChEMBL values

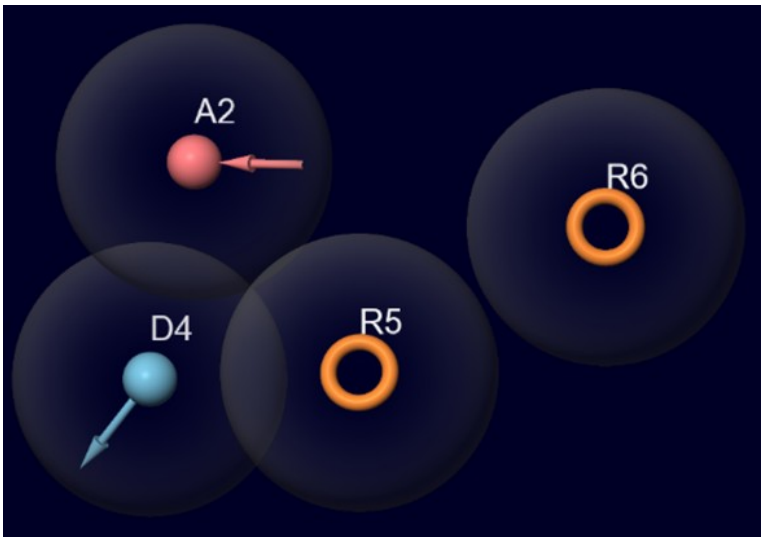

FIGURE 4.2: Key structural features of the obtained model.

that the generated model is likely to perform well in identifying potential NF-κB inhibitors [132]. By combining the survival score with other evaluation parameters, the overall quality and predictive ability of the model were assessed. A visual depiction of the developed model is provided in Figure 4.2.

The pharmacophore model consists of four essential features: one hydrogen bond acceptor region (A2, shown in pink), one hydrogen bond donor (D4, in blue), and two aromatic rings (R5 and R6, in orange). Notably, no excluded volume shell was identified in the model. The measured distances and angles between these key features help define the required spatial arrangement and size of functional groups in a compound. This spatial insight supports the design of new molecules and aids virtual screening of compound libraries. Figure 4.3 illustrates the distances and angles between the pharmacophoric features.

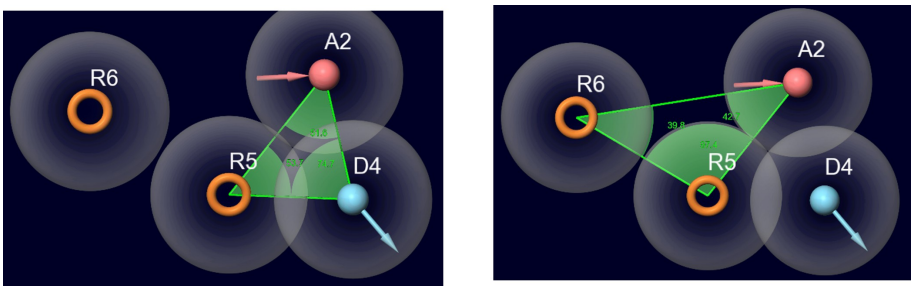

FIGURE 4.3: Angles among the key pharmacophoric features of the hypothesis.

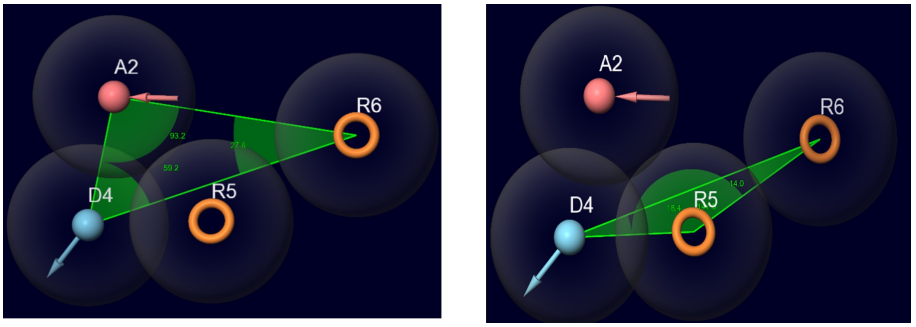

FIGURE 4.4: Angles among the key pharmacophoric features of the hypothesis

The spatial orientation of the pharmacophore features was meticulously analyzed through the various dihedral and bond angles formed between the constituent points represented Figure 4.3 and 4.4. As depicted in the model, the angular relationships between features A2, D4, R5 and R6 varied, providing critical insights into the preferred conformational space for ligand binding.

TABLE 4.1: Angles in among the pharmacophoric features of the hypothesis.

Sr.	**Angle Between (Atoms Order)**	**Angle**	**Sr.**	**Angle Between (Atoms Order)**	**Angle**
1	R5 – A2 – D4	51.6°	2	A2 – R6 – D4	93.2°
3	A2 – R5 – D4	53.7°	4	A2 – D4 – R6	59.2°
5	R5 – D4 – A2	74.7°	6	R6 – A2 – D4	27.6°
7	R6 – A2 – R5	42.7°	8	D4 – R6 – R5	14.0°
9	A2 – R6 – R5	39.8°	10	D4 – R5 – R6	147.6°
11	A2 – R5 – R6	97.4°	12	R5 – D4 – R6	18.4°

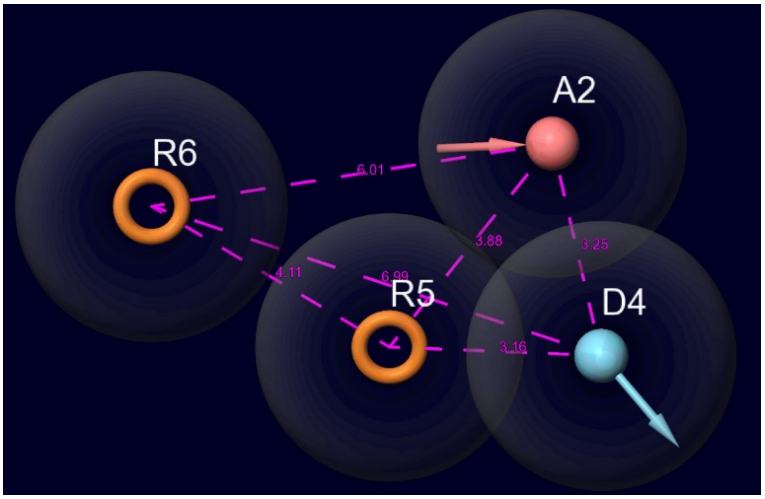

FIGURE 4.5: Distances among the pharmacophoric features of the hypothesis

The inter-feature distances within the developed pharmacophore model delineate the precise spatial separation required for effective molecular recognition. Examination of these distances, measured in Angstroms (A), revealed a defined topological arrangement of the critical interaction points. Specifically, the separation between A2 with D4, R5 and R6 was found to be 3.25, 3.88 and 6.01 A, a common range for interactions such as hydrogen bonding or close contacts between atoms. Distances involving the R5 feature showed notable variations, with R5-D4 at 3.16 A and R5-R6 at 6.99 A, suggesting differential accessibility or interaction types for these points. Furthermore, the R6 feature maintained distinct separations from the other points, evidenced by distances of 6.99 A from D4. These precise distance constraints, alongside the angular data, collectively form the foundation for rational compound design, ensuring that synthesized molecules possess the requisite spatial complementarity to the target's binding pocket.

After aligning all the active compounds used for model generation, it was observed that each compound consistently exhibited all four pharmacophoric features defined in the final hypothesis. These features included one hydrogen bond acceptor, one hydrogen bond donor, and two aromatic rings. This uniform presence across all active molecules supports the reliability of the developed pharmacophore model. The alignment of these compounds with the generated hypothesis is illustrated in Figure 4.6.

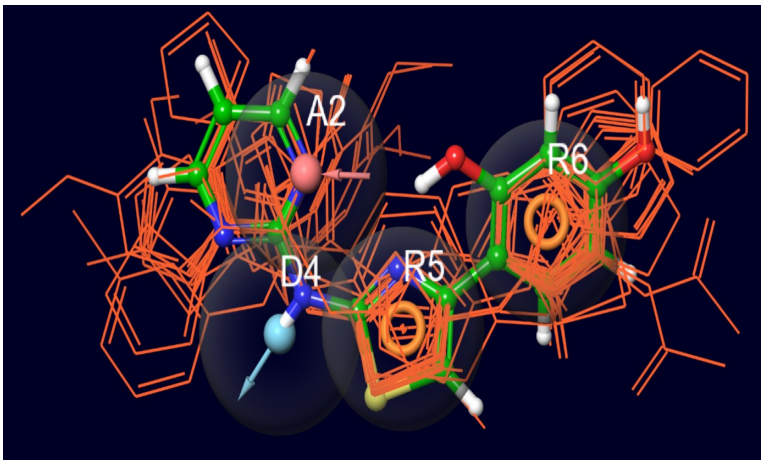

FIGURE 4.6: The aligned ligand with the pharmacophore model

4.3 Validation of Pharmacophore Model

The generated pharmacophore model was rigorously validated to assess its ability to effectively discriminate active compounds from a large dataset of inactives (decoys).

TABLE 4.2: Scoring metrics and explanations

Scoring Metric	**Value**	**Explanation**
PhaseHypoScore	1.306	Cumulative score indicating the pharmacophore hypothesis performance. Higher values reflect better alignment and scoring.
BEDROC 160.9	0.704	Assesses early recognition of actives. A score ¿ 0.7 indicates strong early enrichment, essential for virtual screening.
BEDROC 20.0	0.503	Reflects moderate early enrichment. Value close to 0.5 indicates performance better than random.
BEDROC 8.0	0.488	Shows broader threshold early performance. Slightly lower value still supports predictive capability.

Table 4.2 continued from previous page

Scoring Metric	Value	Explanation
ROC	0.48	Receiver Operating Characteristic curve. Score close to 0.5 shows moderate discrimination between actives and decoys.
RIE	8.69	Robust Initial Enhancement measures early enrichment. Higher values show better early retrieval of actives.
AUC	0.69	Area under the accumulation curve. Indicates faster accumulation of actives than random, showing good performance.
EF 1% (Enrichment Factor)	43	Model retrieved 43x more actives in top 1% than expected by chance — excellent early recognition.
EF 2%, 5%, 10%, 20%	22, 9.6, 4.8, 2.4	Declining trend shows model is most effective at early percentages, as expected.
Total Number of Actives	12	Out of 26 total actives, 12 were retrieved — all ranked in top 1–20%.
Total Number of Ranked Actives	12	All retrieved actives were properly aligned and scored.

For this purpose, a test set comprising 27 known active NF-κB inhibitors and 1650 diverse decoy compounds (totaling 1675 ligands) was utilized.

The model's performance was evaluated using several key metrics, including Receiver Operating Characteristic (ROC) curve analysis, Enrichment Factors (EF), and Boltzmann-Enhanced Discrimination of Receiver Operating Characteristic (BEDROC) scores, as summarized in Table 4.2.

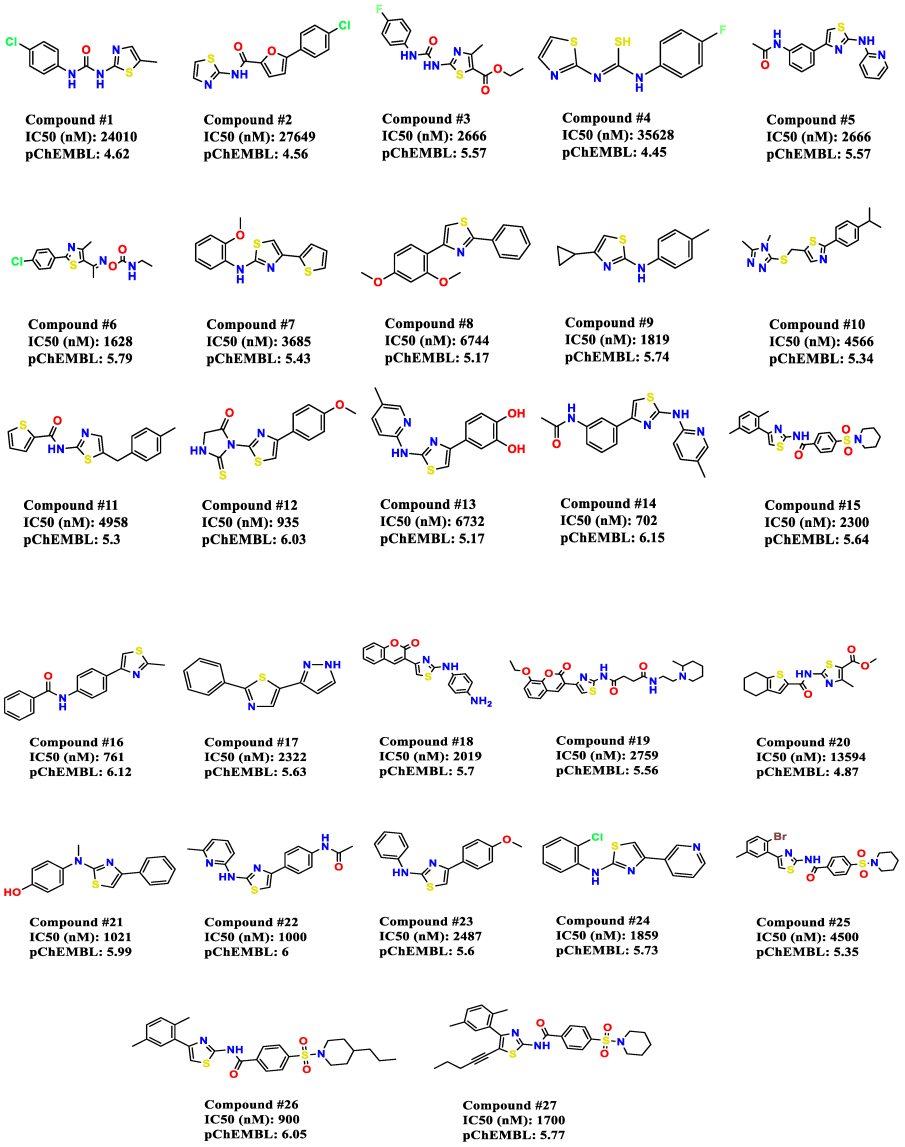

FIGURE 4.7: The chemical structure of molecules of test set

4.4 Design of potential Inhibitors

The potential inhibitor was designed following approach of ligand-based drug design. The criterion for the design of potential inhibitor is mentioned in Chapter 3. MAS-1 (5-benzoyl-N-(4-methoxyphenyl)-2,3-dihydro-1H-pyrrolizine-1-carboxamide), MAS-2 (2-(2-((2,6-dichlorophenyl)amino)phenyl)-N-(p-tolyl)acetamide) and MAS-3 (5-benzoyl-N-(4-nitrophenyl)-2,3-dihydro-1H-pyrrolizine-1-carboxamide) were designed in accordance with the obtained pharmacophore model and is shown in Figure 4.8, 4.9 and 4.10 respectively.

The concept behind designing a potential inhibitor of NF-κB was to design it in a way that it matches maximum features of the pharmacophore model as well as can bind to the amino acid residues of the catalytic domain.

All the designed compounds, MAS-1, MAS-2 and MAS-3 matches 4 out of 4 pharmacophoric features of the pharmacophore model ADRR (Figure 4.8). The aligned ligand structure shows good correspondence with the developed pharmacophore hypothesis ADRR, demonstrating proper spatial fitting of the key chemical features. The A2 hydrogen bond acceptor feature is accurately mapped to the carbonyl oxygen group within the ligand's side chain, aligning precisely with the acceptor vector of the model. The D4 hydrogen bond donor aligns with a secondary amine or NH group, positioned in the correct orientation to form potential hydrogen bonding with the protein target. Moreover, the ligand matches two aromatic rings (R5 and R6), both of which do not overlap perfectly with the hydrophobic π-system of the model, indicating that the aromatic nature of the ligand needs modification for its interaction with the NF-κB binding site. Moreover, the extra carbonyl group in the molecule also has the potential to accept a hydrogen bond.

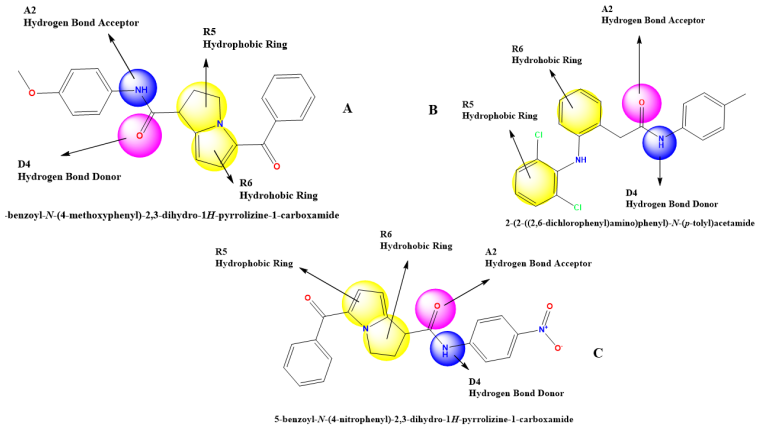

FIGURE 4.8: Ligand-Based features of MAS-1 (A), MAS-2 (B) and MAS-3 (C)

4.5 Molecular Docking and MM-GBSA Analysis

The docking study of the designed compound was performed, using Maestro Glide Module, against the NF-κB protein using the crystal structure with PDB ID:

7VUP. The results indicated favorable binding within the active site of NF-κB by the MAS-3. The XP Glide Score obtained for the designed compound MAS-1, MAS-2 and MAS-3 was -2.958, -3.306 and -5.024 kcal/mol respectively, suggesting a moderate-to-good binding affinity especially with MAS-3.

The Glide Emodel Score for the designed compound MAS-1, MAS-2 and MAS-3 was -44.648, -47.85 and -57.59 respectively, indicating strong stabilization of the ligand inside the protein's binding pocket with minimal internal strain.

The MM-GBSA ΔG Bind energy of MAS-1. MAS-2 and MAS-3 were found to be -28.99, -31.45 and -39.38 kcal/mol respectively, further confirmed the strong binding interaction, as values more negative than -30 kcal/mol typically reflect good binding stability , represented in Figure 4.9-4.11. .

In addition to numerical scores, the ligand–protein interaction diagram provided further structural insights. The designed compound MAS-3 formed multiple important interactions within the NF-κB binding pocket.

Notably, ARG158 formed a hydrogen bond with the carbonyl oxygen of the ligand, while also participating in a -cation interaction with the aromatic ring. Several other residues, including ARG160 and ARG193, contributed to stabilizing the ligand via hydrogen bonding. Several hydrophobic residues such as LEU117, ILE119, LEU154, and LEU181—lined the binding pocket, forming a non-polar environment that helped in anchoring the ligand.

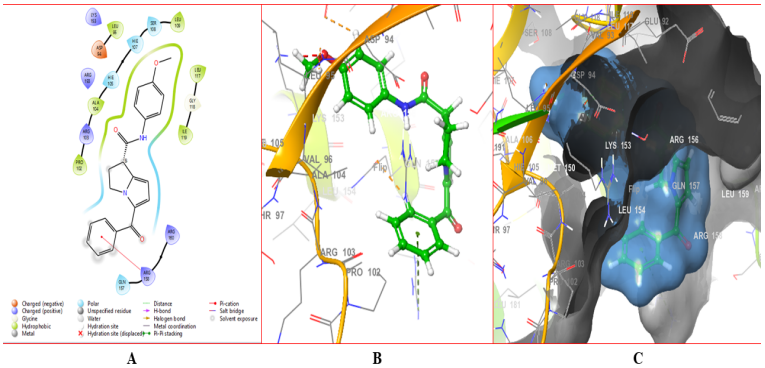

FIGURE 4.9: 2D LID of designed MAS-1 with 7VUP (A), 3D LID of MAS-1 with 7VUP (B), Binding free energy of MAS-1 with 7VUP (C).

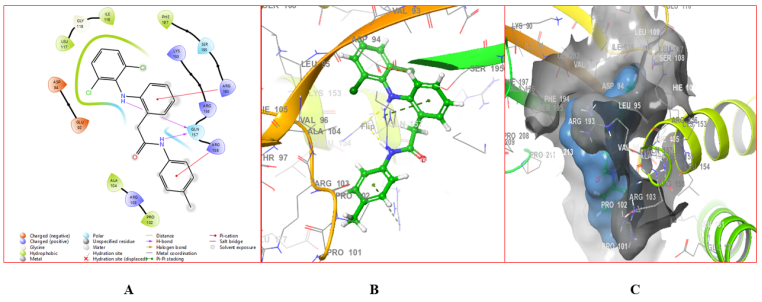

FIGURE 4.10: 2D LID of designed MAS-2 with 7VUP (A), 3D LID of MAS-2 with 7VUP (B), Binding free energy of MAS-2 with 7VUP (C)

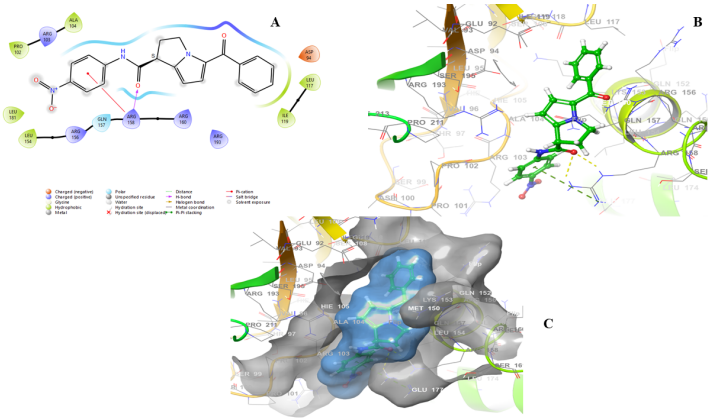

FIGURE 4.11: 2D LID of designed MAS-3 with 7VUP (A), 3D LID of MAS-3 with 7VUP (B), Binding free energy of MAS-3 with 7VUP (C).

The ligand also displaced a hydration site near ARG158, which may contribute to favorable binding by replacing energetically less favorable water molecules. The presence of multiple charged and polar residues such as ARG103, ARG156, and GLN157 further suggests that the ligand is well accommodated within the binding site through a combination of polar, electrostatic, and hydrophobic interactions. The 2D, 3D and Binding Free Energy of LID of designed compound with NF-κB protein (PDB ID: 7VUP) are shown in Figure 4.9 A, B, C respectively.

To validate the reliability of the pharmacophore model used to design the compound, five random test set compounds were selected and docked against the same NF-κB protein structure (PDB ID: 7VUP). These compounds showed a range of binding behaviors, confirming the selectivity of the designed ligand as shown in table 4.3.

TABLE 4.3: Molecular Docking and MM-GBSA Scores for Designed Inhibitor and Randomly Selected Test Set Compounds against NF-κB (PDB ID: 7VUP).

Compound	**XP Glide Score (kcal/mol)**	**Emodel Score**	**MM-GBSA dG-bind (kcal/mol)**
MAS-1	-2.958	-44.648	-28.99
MAS-2	-3.306	-47.850	-31.45
MAS-3	-5.024	-57.590	-39.38
Compound 5	-3.084	-42.539	-31.384
Compound 4	-2.833	-39.541	-16.301
Compound 3	-2.767	-38.792	-12.981
Compound 2	-2.389	-44.429	-33.130
Compound 1	-0.708	-42.174	-25.809

These findings collectively validate the pharmacophore model used for virtual screening and compound design. The designed compound MAS-3 demonstrated superior binding affinity, better docking pose stability, and stronger protein–ligand interactions when compared to the test set. The validation step using the test compounds helped confirm that the pharmacophore model was selective and capable of prioritizing a compound with significantly improved binding characteristics. This supports the potential of the MAS-3 as a lead NF-κB inhibitor for further development in anti-Alzheimer's research.

4.6 Molecular Dynamic Simulations

4.6.1 Protein-Ligand Interaction Profile

The protein-ligand interaction analysis revealed several key binding interactions throughout the simulation trajectory (Figure 4.13). The ligand, containing a nitrobenzene moiety connected to a complex heterocyclic scaffold, established multiple contact points with the NF-κB binding pocket. Notably, the interaction with arginine residue 166 (ARG166) showed significant stability, with approximately 14% occupancy throughout the simulation period.

The presence of the nitro group appears to be crucial for maintaining electrostatic interactions with positively charged residues in the binding site. This observation is consistent with previous studies highlighting the importance of electrostatic complementarity in protein-ligand recognition.

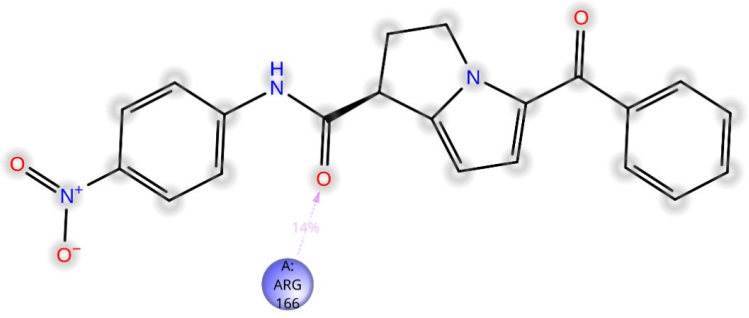

FIGURE 4.12: Pictorial representation of atomic contributors in ligand protein complex.

4.6.2 Amino Acid Interaction Frequency Analysis

The interaction frequency analysis across all amino acid residues (Figure 4.13) demonstrates that the ligand establishes contacts with multiple residues within the NF-κB binding pocket. The highest interaction frequencies were observed with residues located in the central binding region, suggesting that the ligand occupies a well-defined binding pose.

The distribution of interaction frequencies indicates that the ligand does not rely on a single dominant contact but rather forms a network of weaker interactions that collectively contribute to binding stability. This interaction profile is characteristic of drug-like molecules that exhibit favorable binding kinetics and reduce susceptibility to resistance mutations.

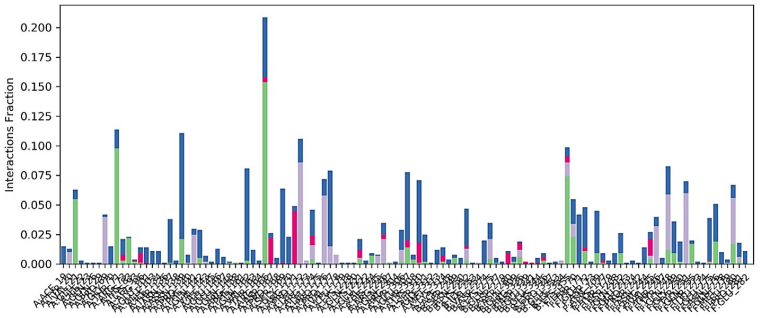

FIGURE 4.13: The interaction fraction of all the amino acid residues with the ligand atoms

4.6.3 Structural Stability and Contact Analysis

The contact map analysis (Figure 4.14) provides a comprehensive view of the temporal evolution of protein-ligand contacts throughout the 200-nanosecond simulation. The data reveals several distinct phases of binding:

Initial Binding Phase (0-25 ns): The ligand undergoes rapid conformational adjustment within the binding pocket, establishing initial contacts with nearby residues.

Stabilization Phase (25-100 ns): A more stable interaction pattern emerges, with consistent contact formation across multiple residues.

Equilibrium Phase (100-200 ns): The interaction pattern reaches a steady state, with periodic fluctuations reflecting the dynamic nature of the binding interface.

The total contact count (upper panel) remained relatively stable throughout the simulation, averaging between 2-4 contacts at any given time. This suggests that the ligand maintains consistent engagement with the binding pocket without excessive mobility that would indicate unstable binding.

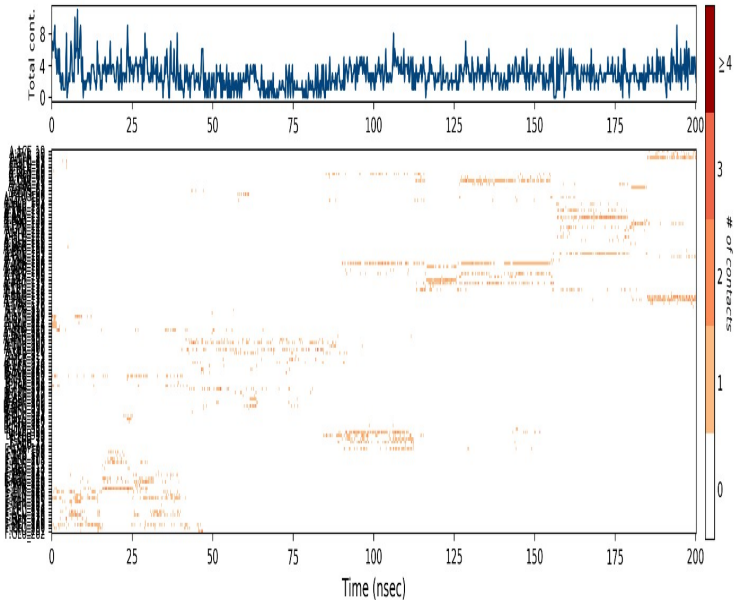

FIGURE 4.14: Interaction between amino acids and the ligand throughout the simulation period

4.6.4 Protein and Ligand RMSD Analysis

The RMSD analysis (Figure 4.15) provides critical insights into the structural stability of both the protein backbone and the ligand throughout the simulation. The protein RMSD (blue line) shows an initial rapid increase during the first 25 nanoseconds, reaching approximately 17 Å before stabilizing. This initial increase likely reflects necessary conformational adjustments to accommodate ligand binding.

Following the initial equilibration period, the protein RMSD exhibits a gradual increase, reaching a plateau around 150 nanoseconds. This behavior suggests that the protein undergoes conformational changes that are stabilized by ligand binding, a phenomenon commonly observed in induced-fit binding mechanisms.

The ligand RMSD (red line) displays more pronounced fluctuations throughout the simulation, with values ranging from approximately 20 to 60 Å. These fluctuations are the result of intrinsic disordered protein nature of different dimers of the simulation NF-κB. The high ligand RMSD values may indicate either significant conformational flexibility of the ligand or possible binding site transitions. The

correlation between protein and ligand RMSD values in certain regions suggests coordinated conformational changes that may be functionally relevant.

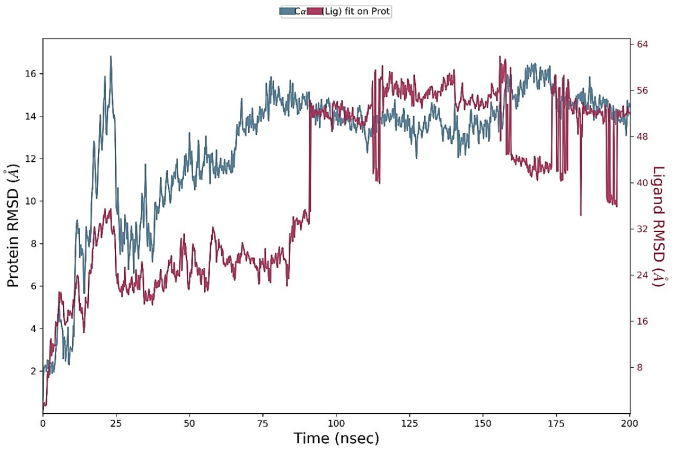

FIGURE 4.15: RMSD of both Apo form and ligand protein complex

The combined analysis of interaction profiles, contact maps, and RMSD data suggests that the ligand binding follows an induced-fit mechanism. The initial protein conformational changes, evidenced by the rapid RMSD increase, are followed by a period of mutual adaptation between the protein and ligand. This mechanism is consistent with the flexible nature of transcription factor binding sites, which often undergo conformational changes upon ligand binding.

The sustained interaction with ARG166 throughout the simulation highlights the importance of this residue in ligand recognition. This arginine residue may serve as an anchor point, providing electrostatic stabilization while allowing for conformational adjustments in other regions of the binding interface.

4.7 ADMET Profiling

The ADMET (Absorption, Distribution, Metabolism, Excretion, and Toxicity) profiling of MAS-1, MAS-3, and MAS-2 provides critical insights into their potential as drug candidates as per table 4.4.

4.7.1 Absorption

All three compounds exhibit high absorption risks, with MAS-2 showing the highest at 93%, followed by MAS-3 at 86%, and MAS-1 at 84%. These risks are likely influenced by their physicochemical properties, particularly their lipophilicity and solubility. MAS-2 has the highest lipophilicity, with LogP and LogD values of 5.726, compared to 3.298 for MAS-1 and 3.226 for MAS-3. High lipophilicity often correlates with poor water solubility, which is evident across all compounds. MAS-3 has the lowest water solubility (0.0001707 mg/mL), followed by MAS-2 (0.001 mg/mL) and MAS-1 (0.002 mg/mL). Passive transcellular permeability, measured by PAMPA, is high for MAS-1 (96%) and MAS-2 (92%), indicating good potential for oral absorption through passive diffusion. In contrast, MAS-3's low PAMPA permeability (43%) suggests challenges in passive absorption, which could limit its bioavailability. However, MDCK permeability, which includes both transcellular and paracellular routes, shows MAS-2 with the highest permeability ($1720.949 cm/sx10^7$), followed by MAS-1 (595.364 cm/s x 10^7)$and MAS-3$(437.217 cm/s x 10^7). This suggests that MAS-3 may still achieve reasonable absorption through alternative mechanisms despite its low passive permeability. The effective human jejunal permeability (S+Peff) further supports this, with MAS-2 (4) and MAS-1 ($4.051 cm/sx10^4$) outperforming MAS-3 (4

4.7.2 Distribution

The fraction unbound in human plasma ($hum_fup\%$) varies significantly among the compounds. MAS-2 has the lowest fraction unbound (1.736%), indicating high protein binding, which may restrict its distribution to tissues and affect its pharmacokinetics. MAS-1 (3.597%) and MAS-3 (4.992%) have higher fractions unbound, suggesting better availability for tissue distribution. The volume of distribution (Vd) reflects these differences, with MAS-2 having the highest Vd (2.123 L/kg), indicating wider distribution in the body, likely due to its high lipophilicity. MAS-1 (1.346 L/kg) and MAS-3 (1.212 L/kg) have lower Vd values, suggesting more limited distribution. The blood-brain barrier (BBB) penetration,

indicated by LogBB, shows MAS-2 with the highest potential to cross the BBB (0.377), followed by MAS-3 (-0.133) and MAS-1 (-0.364). However, MAS-2's status as a P-glyc Stufe an Pgp substrate may limit its brain penetration, as discussed below.

4.7.3 Metabolism and Excretion

Specific metabolism data for MAS-1, MAS-3, and MAS-2 was not available in the provided attachments. However, the physicochemical data indicates that all three compounds are primarily cleared by metabolism, as predicted by the $S + CL_Mech$ parameter, with no significant renal or hepatic uptake clearance. Their high LogP values suggest they may be substrates for cytochrome P450 enzymes, particularly those that metabolize lipophilic compounds. Further studies are needed to elucidate their specific metabolic pathways and potential drug-drug interactions.

4.7.4 Toxicity

The toxicity profiles of the three compounds reveal significant differences that could impact their safety as drug candidates.

Androgen Receptor Toxicity: All three compounds are predicted to be toxic to the androgen receptor, with MAS-3 having the highest probability (71%), followed by MAS-1 and MAS-2 (59%). This suggests potential endocrine-disrupting effects, which could pose challenges for reproductive health safety.

hERG Channel Blockade: MAS-2 is the only compound predicted to block the hERG potassium channel (Yes, 61%), a significant concern due to the risk of QT prolongation and cardiotoxicity. MAS-1 (No, 73%) and MAS-3 (No, 91%) are not predicted to block hERG, making them safer in this regard.

Acute Toxicity: Acute rat toxicity, measured by LD50, is lowest for MAS-2 (793.134 mg/kg), indicating it is the most acutely toxic, while MAS-3 is the least toxic (1820.878 mg/kg), and MAS-1 is intermediate (1026.875 mg/kg).

Reproductive Toxicity: All three compounds are predicted to be reproductively toxic, with MAS-3 and MAS-2 at higher risk (90%) compared to MAS-1 (68%).

Skin Sensitization: MAS-1 is predicted to be non-sensitizing (67%), while MAS-3 (90%) and MAS-2 (74%) are sensitizers, with MAS-3 having the highest probability.

Mutagenicity: Mutagenicity risk is highest for MAS-3 (1.8), followed by MAS-2 (0.9) and MAS-1 (0.6). MAS-3's higher risk is driven by positive predictions in multiple Ames test strains (TA100, TA97, TA98, and NIHS panel).

Overall Toxicity Risk: The overall toxicity risk is lowest for MAS-1 (0), followed by MAS-2 (0.521) and MAS-3 (1.5), indicating MAS-1 has the fewest predicted toxicity issues.

4.7.5 Transporter Interactions

Transporter interactions play a critical role in pharmacokinetics and drug safety.

Breast Cancer Resistance Protein (BCRP): MAS-1 (Yes, 64%) and MAS-2 (Yes, 50%) are predicted to be BCRP substrates, which may reduce their oral bioavailability due to efflux. MAS-3 is not a BCRP substrate (No, 63

Bile Salt Export Pump (BSEP): All three compounds inhibit BSEP, with MAS-1 and MAS-2 at 83% and MAS-3 at 59%. BSEP inhibition is associated with cholestatic liver injury, a significant safety concern.

Organic Anion Transporter 3 (OAT3): All three compounds inhibit OAT3, with MAS-2 showing the highest inhibition (93%), followed by MAS-3 (74%) and MAS-1 (70%). MAS-1 (55%) and MAS-3 (74%) are OAT3 substrates, while MAS-2 is not (No, 72%). OAT3 inhibition may affect the renal excretion of co-administered drugs.

P-glycoprotein (Pgp): MAS-1 and MAS-2 inhibit Pgp (Yes, 62%), while MAS-3 does not (No, 76%). MAS-2 is a Pgp substrate (Yes, 72%), which may limit its

brain penetration and affect tissue distribution, while MAS-1 and MAS-3 are not Pgp substrates (No, 74% and 55%, respectively).

MAS-1 appears to be the most promising candidate due to its lower toxicity risks, including no hERG blockade, non-sensitizing skin properties, and the lowest mutagenicity and overall toxicity risks. However, its high absorption risk and low solubility require optimization. MAS-3, while less acutely toxic, has higher reproductive toxicity and mutagenicity risks, and its low PAMPA permeability may hinder absorption. MAS-2's high lipophilicity, hERG blockade, and Pgp substrate status pose significant safety and pharmacokinetic challenges. The absence of metabolism data necessitates further studies to confirm their metabolic profiles. In vitro and in vivo experiments are recommended to validate these predictions and optimize their pharmacokinetic properties.

Table 4.4: Comparative Table of ADMET profiles of MAS-1, MAS-2 and MAS-3.

Parameter	**MAS-1**	**MAS-2**	**MAS-3**
Absorption Risk	High (84%)	High (93%)	High (86%)
S+logP	3.298	5.726	3.226
S+Sw (mg/mL)	0.002	0.001	0.0001707
hum_fup%	3.60%	1.74%	4.99%
Vd (L/kg)	1.346	2.123	1.212
LogBBB	-0.364	0.377	-0.133
Andro Filter	Toxic (59%)	Toxic (59%)	Toxic (71%)
hERG Filter	No (73%)	Yes (61%)	No (91%)
Rat Acute (mg/kg)	1026.875	793.134	1820.878
Repro Tox	Toxic (68%)	Toxic (90%)	Toxic (90%)
Sens Skin	Nonsensit. (67%)	Sensitizer (74%)	Sensitizer (90%)
MUT Risk	0.6	0.9	1.8
TOX Risk	0	0.521	1.5
Pgp Substr	No (74%)	Yes (72%)	No (55%)
OAT3 Inh	Yes (70%)	Yes (93%)	Yes (74%)
OAT3 Substr	Yes (55%)	No (72%)	Yes (74%)

4.7.6 BCS Classification Analysis

The Biopharmaceutics Classification System (BCS) analysis for MAS-1, MAS-2, and MAS-3 as Figure 4.16 illustrate, based on their solubility and permeability, classifies all three compounds as BCS Class II (low solubility, high permeability). Solubility values are 0.002 mg/mL for MAS-1, approximately 0 mg/mL (noted as 0.0001707 mg/mL from prior data) for MAS-3, and 0.001 mg/mL for MAS-2, all falling below the high solubility threshold where Dose/Solubility 250 mL. At the highest dose of 500 mg, the Dose/Solubility ratios are 250,000 mL for MAS-1, approximately 2,929,000 mL for MAS-3, and 500,000 mL for MAS-2, confirming low solubility. Permeability values—4.051 × 10 cm/s for MAS-1, 1.988 × 10 cm/s for MAS-3, and 4.631 × 10 cm/s for MAS-2—all exceed the high permeability threshold of 1 × 10 cm/s. This classification indicates that absorption is limited by dissolution rate, necessitating formulation strategies to enhance solubility for improved bioavailability.

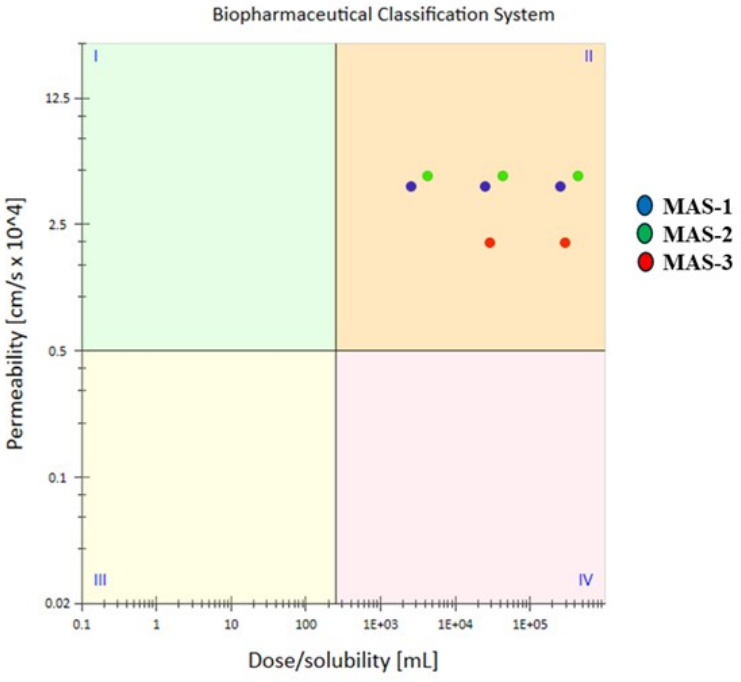

FIGURE 4.16: BCS Classification of MAS-1, MAS-2 and MAS-3

4.8 Characterization

4.8.1 FTIR Spectroscopic Analysis

Fourier Transform Infrared (FTIR) spectroscopy was employed to confirm the formation of an amide in all three products, MAS-1, MAS-2 and MAS-3. Summarize in table 4.7.

4.8.1.1 MAS-1 FT-IR characterization

MAS-1 demonstrates characteristic amide functionality through the presence of a distinct amide I band at 1699 cm^{1} corresponding to C=O stretching, complemented by amide II bands at 1643 and 1530 cm^{1} representing N-H bending coupled with C-N stretching vibrations, alongside broad N-H stretching at 3300-3500 cm^{1}. The compound also exhibits the expected benzoyl ketone carbonyl at 1789 cm^{1} and methoxy group C-O stretching at 1021 cm^{1}, confirming the structural integrity of the pyrrolizine-methoxyphenyl amide as in Figure 4.17.

4.8.1.2 MAS-2 FT-IR characterization

MAS-2 similarly displays clear amide characteristics with the amide I band appearing at 1729 cm^{1} and amide II bands at 1610 and 1545 cm^{1}, supported by broad N-H stretching in the 3000-3500 cm^{1} region, represented in Figure 4.18. The spectrum additionally shows characteristic C-Cl stretching vibrations at 827 and 745 cm^{1}, confirming the presence of the dichlorophenyl moiety, while the aromatic amine C-N stretching at 1300 cm^{1} validates the diclofenac-tolyl amide structure.

4.8.1.3 MAS-3 FT-IR characterization

MAS-3 exhibits amide I band at 1643 cm^{1} with broad N-H stretching at 3805-3570 cm^{1}, confirming amide bond formation. The presence of the benzoyl ketone at 1871 cm^{1} and the characteristic nitro group asymmetric N-O stretching at 1530 cm^{1},

along with aromatic vibrations at 1408 and 1386 cm^1, conclusively demonstrates the successful synthesis of the pyrrolizine-nitrophenyl amide.

The consistent appearance of amide I and II bands across all three compounds, coupled with their respective substituent-specific vibrational signatures, provides robust spectroscopic evidence for the successful formation of the target amide linkages in each molecule as in Figure 4.19.

4.8.2 NMR Spectroscopic Analysis

4.8.2.1 ^{13}C NMR spectrum of MAS-3

The ^{13}C NMR spectrum displayed characteristic chemical shift values corresponding to distinct carbon frameworks, providing critical structural insights into product.

The interpretation of the ^{13}C NMR data for product synthesized is provided in Table 4.8. The spectrum of ^{13}C NMR is also illustrated in Figure 4.22. The ^{13}C NMR spectrum shows that the molecule has a few different carbons atmospheres.

The two benzene rings contributed signals in the 119.6, 125.8, 126.8 and 128.8 ppm range. Ring A, substituted with a carbonyl with ortho and para carbons deshielded (136.0 ppm) due to the electron-withdrawing effect, and meta carbons slightly upfield (120–130 ppm).

Ring D, with a nitro group, with the carbon attached to -NO significantly deshielded (139.5 ppm) due to the strong electron-withdrawing nature. The ketonic carbonyl C=O appears at 136.0 ppm amide carbonyl C-NH2 connected to Ring A and pyrrolidine appeared at 162.8 ppm confirming the product formation.

The interpretation of the ^{13}C NMR data for product synthesized is provided in Table 4.8. The spectrum of ^{13}C NMR is also illustrated in Figure 4.22. The ^{13}C NMR spectrum shows that the molecule has a few different carbons atmospheres.

Table 4.5: FTIR Analysis of Amide Compounds with Main Peaks and Functional Groups

Wavenumber (cm^{-1})	**MAS-1**	**MAS-2**	**MAS-3**	**Functional Group**	**Interpretation**
3500–3200	3300–3500 (broad)	3000–3500 (broad)	3805–3570 (broad)	N–H stretch	Primary and secondary amide N–H stretching
1800–1750	1789	–	1871	C=O stretch (ketone)	Benzoyl carbonyl group
1700–1650	1699	1729	1643	C=O stretch (amide I)	Amide carbonyl stretching
1650–1600	1643	1610	–	Amide II band	N–H bending + C–N stretching
1600–1500	1530	1545	–	Amide II band	Secondary amide N–H bending
1500–1400	1405	1487, 1457	1408, 1386	Aromatic C=C stretch	Aromatic ring vibrations

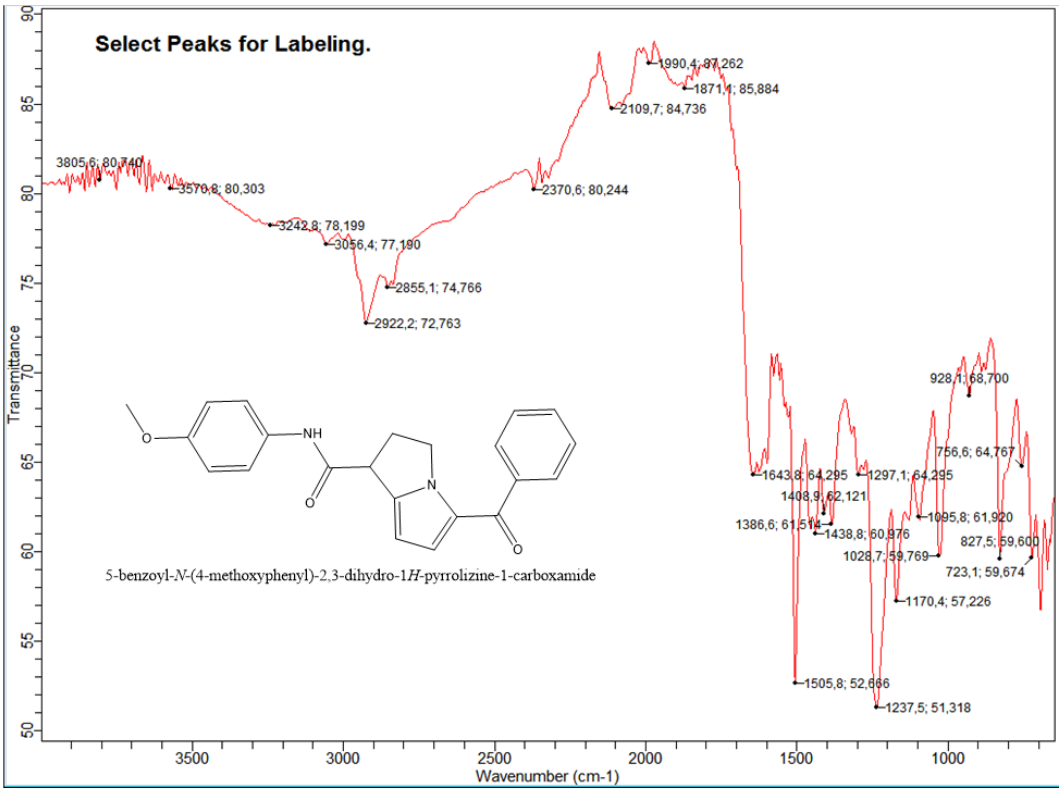

FIGURE 4.17: Graphical representation of FTIR spectral data of product MAS-1

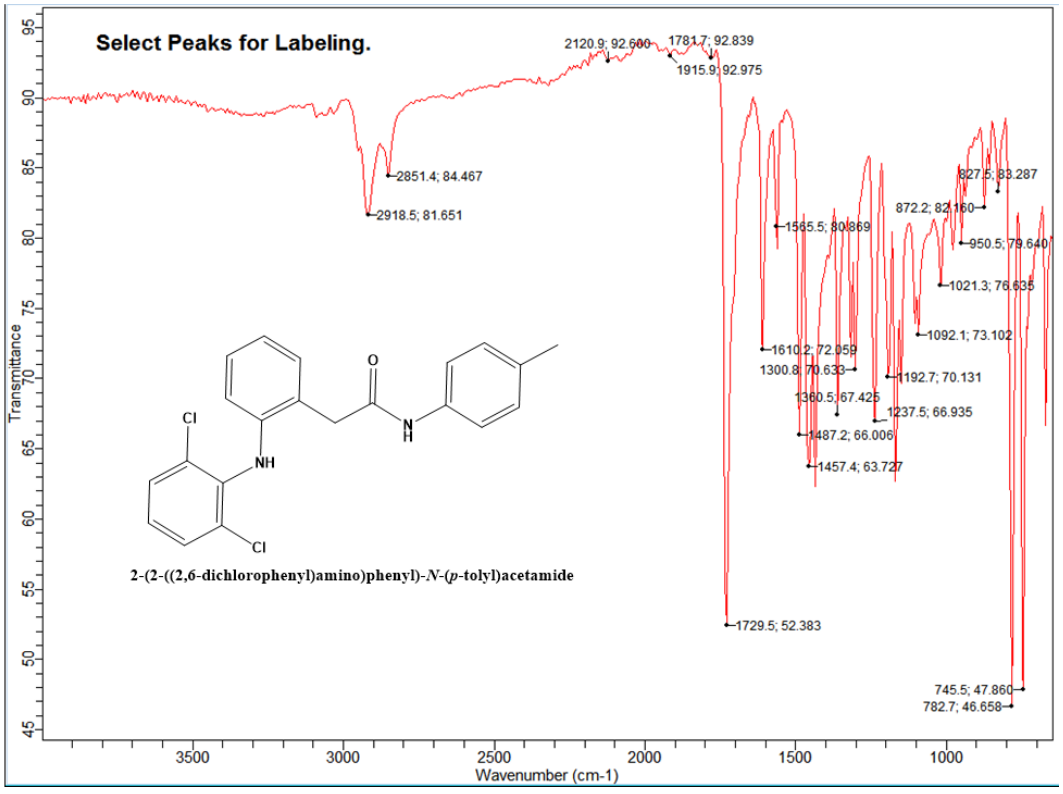

FIGURE 4.18: Graphical representation of FTIR spectral data of product MAS-2.

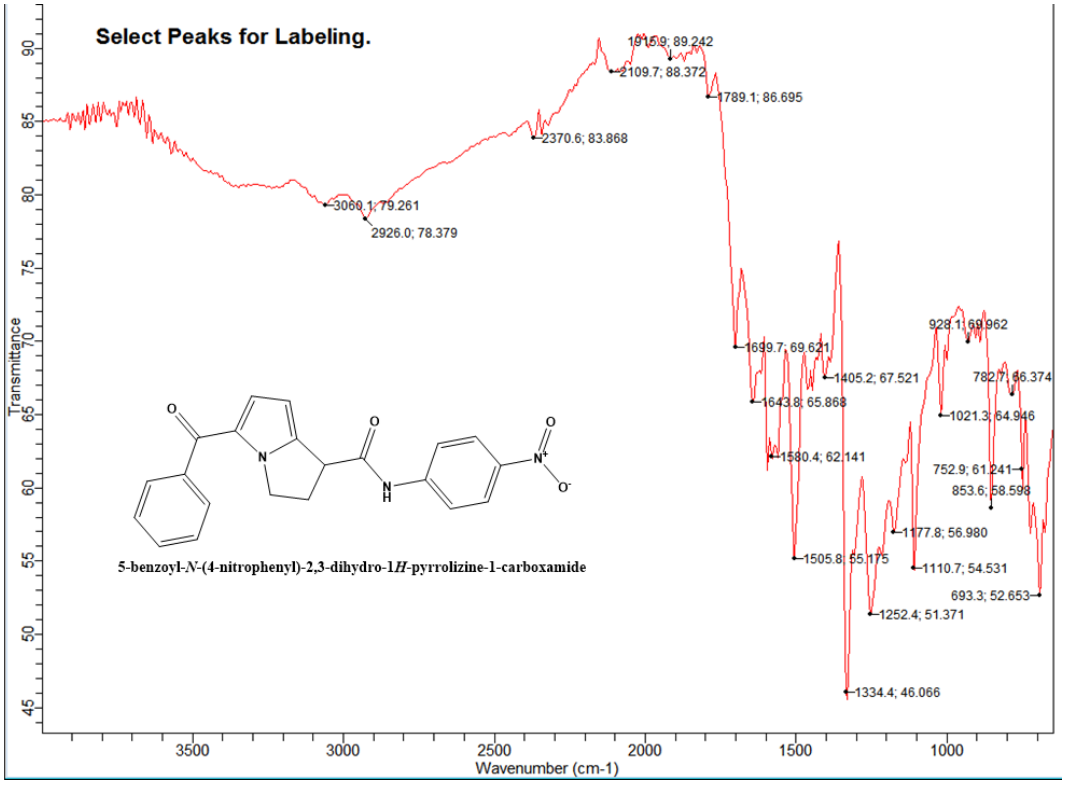

FIGURE 4.19: Graphical representation of FTIR spectral data of product MAS-3.

TABLE 4.6: Interpretation of MAS-3 by ^{13}C NMR spectrum

Carbon Type / Position	**Chemical Shift (ppm)**
–CH / –CH (aliphatic region)	31.2, 34.6, 36.3
Heterocyclic ring carbons (C=C / C–N)	107.4, 112.9
Aromatic CH carbons	119.6, 125.8, 126.8, 128.8
Quaternary aromatic carbon (C–NO)	139.5
Amide carbonyl	162.8
Ketonic carbonyl (C=O)	136.0

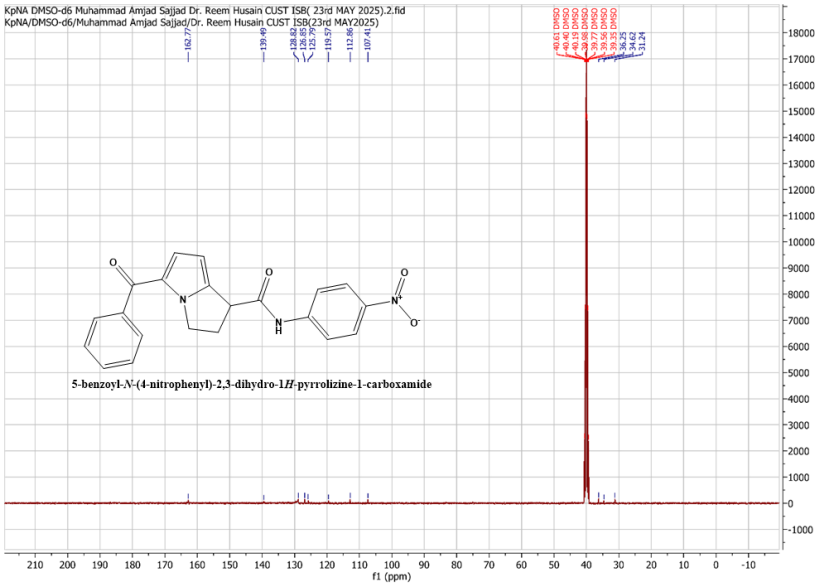

FIGURE 4.20: C-13 NMR spectral representation of MAS-3 ^{13}C NMR

4.8.2.2 ^{1}H-NMR Spectrum Interpretation of MAS-3

The proton NMR spectrum of 5-benzoyl-N-(4-nitrophenyl)-2,3-dihydro-1H-pyrrolizine-1-carboxamide was recorded in DMSO-d using a 400 MHz spectrometer. The spectrum showed well-resolved aromatic and aliphatic proton signals, which were consistent with the proposed molecular structure.

In the aromatic region, several signals appeared between Δ 8.34 and 6.60 ppm. A doublet at Δ 8.34 ppm (J = 9.2 Hz) and another at Δ 7.82 ppm (J = 9.2 Hz) were assigned to the ortho-coupled protons of the para-substituted nitrophenyl ring. Two singlets at Δ 8.21 ppm and Δ 7.95 ppm correspond to aromatic protons that are deshielded due to their proximity to the amide and carbonyl groups.

The group of peaks between Δ 7.75–7.47 ppm (integrating for five protons) represents the protons of the benzoyl phenyl ring. Additional aromatic resonances observed at Δ 6.97 ppm (d, J = 7.0 Hz) and Δ 6.60 ppm (d, J = 9.2 Hz) were attributed to protons within the pyrrolizine ring system.

In the aliphatic region, characteristic peaks appeared between Δ 3.40 and 2.72 ppm, confirming the presence of methylene protons in the dihydropyrrolizine ring. A doublet at Δ 3.40 ppm (J = 12.9 Hz), along with singlets at Δ 3.18 ppm

and Δ 2.88 ppm, correspond to the non-equivalent methylene protons adjacent to nitrogen and carbonyl atoms. The multiplet observed at Δ 2.73–2.72 ppm further supports the presence of the dihydropyrrolizine framework. Overall, the proton NMR data clearly support the expected structure of the compound. The chemical shifts and splitting patterns match the predicted environment of aromatic, amide, and aliphatic protons, confirming the successful formation of the target molecule.

TABLE 4.7: 1H NMR spectrum of MAS-3 with integration results and depiction of multiplicity.

Chemical Shift δ(ppm)	**Multiplicity**	**Integration**	**J (Hz)**
6.765	Doublet (d)	2H	4.0
6.970	Doublet (d)	1H	8.0
7.575	Doublet (d)	2H	4.0
7.505	Doublet (d)	2H	4.0
7.750	Triplet (t)	3H	8.0
7.782	Doublet (d)	2H	8.0
8.980	Singlet (s)	1H	–

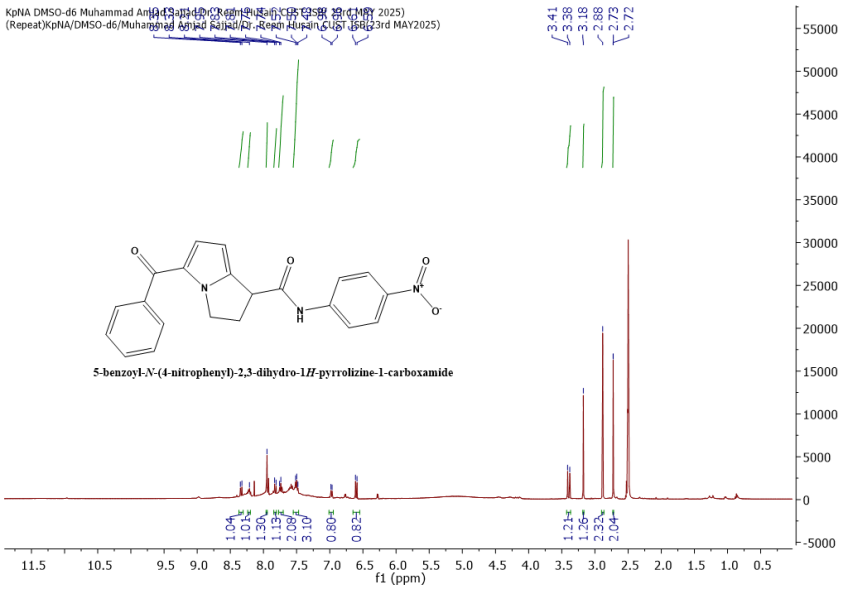

FIGURE 4.21: H-NMR spectral representation of MAS-3 by H NMR

4.9 Biological Evaluation

4.9.1 Antioxidant DPPH Assay

The antioxidant potential of the synthesized compounds MAS-1, MAS-2, and MAS-3 were evaluated using the DPPH (2,2-diphenyl-1-picrylhydrazyl) with Ascorbic acid as Positive control for free radical scavenging assay. The results demonstrated that MAS-3 exhibited the highest antioxidant activity among the three compounds tested (Figure 4.24). At the highest concentration of 200 μg/ml, MAS-3 showed remarkable free radical scavenging activity with 90.9% inhibition. This activity remained substantial at lower concentrations, displaying 49.9% scavenging at 66.66 µg/ml, 32.3% at 22.22 µg/ml, and 8.0% at 7.40 µg/ml. The dose-dependent response observed for MAS-3 indicates a strong correlation between concentration and antioxidant effectiveness when compared to Ascorbic acid standard. In contrast, MAS-1 and MAS-2 showed considerably lower antioxidant activities across all tested concentrations. MAS-1 demonstrated moderate activity with 19.9% scavenging at 200 µg/ml, which decreased to 2.1% at 66.66 µg/ml, 10.1% at 22.22 µg/ml, and 0.5% at the lowest concentration. MAS-2 exhibited the weakest antioxidant response, showing only 12.7% scavenging at 200 µg/ml, 9.3% at 66.66 µg/ml, 3.5% at 22.22 µg/ml, and 1.1% at 7.40 µg/ml.

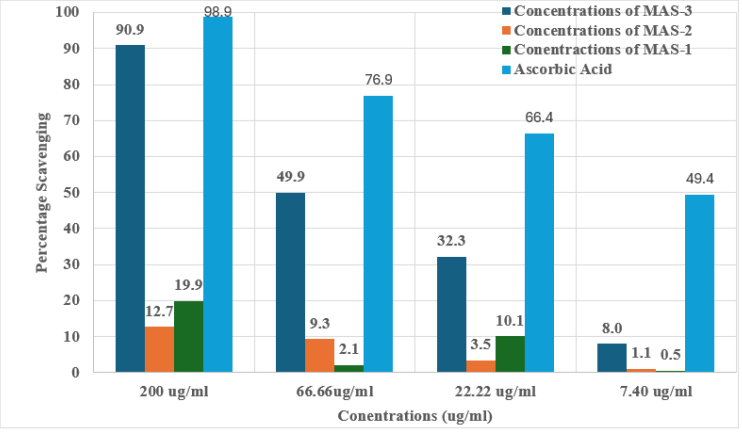

FIGURE 4.22: Percentage Free radical scavenging of the synthesized compounds at different concentrations

The superior antioxidant activity of MAS-3 can be attributed to the presence of the nitrophenyl group in its structure, which may enhance electron donation capacity and stabilize free radicals more effectively than the methoxyphenyl group in MAS-1 or the tolyl group in MAS-2. The results indicate that MAS-3 possesses significant potential as an antioxidant agent, while MAS-1 and MAS-2 show limited free radical scavenging capabilities under the tested conditions. The strong antioxidant activity of the MAS-3 compound suggests its potential to effectively scavenge reactive oxygen species (ROS), thereby helping to slow down the progression of Alzheimer's disease [122].

4.9.2 Brine Shrimps Lethality Assay

The cytotoxic potential of the synthesized compounds MAS-1, MAS-2, and MAS-3 was evaluated using the brine shrimp lethality assay against *Artemia salina nauplii*. The compounds were tested at four different concentrations (1, 0.5, 0.25, and 0.125 mg/ml) with doxorubicin as a positive control and DMSO as a negative control. The assay was conducted in triplicate under controlled conditions at 34°C for 24 hours.

TABLE 4.8: Percentage lethality of synthesized compounds MAS-1, MAS-2, and MAS-3 against *Artemia salina* nauplii at different concentrations

Sample	**1 µg/mL**	**0.5 µg/mL**	**0.25 µg/mL**	**0.125 µg/mL**
MAS-3	24.3 ± 2.8%	12.5 ± 3.1%	10.4 ± 2.7%	7.9 ± 2.3%
MAS-2	36.4 ± 3.9%	18.8 ± 3.3%	10.3 ± 2.9%	7.6 ± 2.1%
MAS-1	31.9 ± 2.9%	16 ± 3.6%	9.5 ± 2.7%	6.8 ± 2.2%
DMSO	Nil	Nil	Nil	Nil
Doxorubicin	80 ± 5%	71 ± 6%	60 ± 5%	52 ± 3%

All experiments were performed in triplicate, and values are presented as mean ± standard deviation (SD).

The results demonstrated that all three synthesized compounds exhibited moderate cytotoxic activity against brine shrimp nauplii in a dose-dependent manner (Table 4.10). MAS-2 showed the highest lethality with 36.4 ± 3.9% mortality at the maximum concentration of 1 mg/ml, followed by MAS-1 with 31.9 ± 2.9% lethality, while MAS-3 displayed the lowest cytotoxic effect with 24.3 ± 2.8% mortality at the same concentration. The cytotoxic activity of all compounds decreased proportionally with decreasing concentrations, showing 12.5-18.8% lethality at 0.5 mg/ml and converging to similar levels (9.5-10.4%) at 0.25 mg/ml. At the lowest concentration of 0.125 mg/ml, all compounds showed minimal cytotoxic effects ranging from 6.8-7.9%.

The positive control doxorubicin demonstrated significantly higher cytotoxicity with 80 ± 5% lethality at 1 mg/ml, confirming the validity of the assay system. The negative control DMSO showed no lethality at any concentration, indicating that the observed effects were specifically due to the test compounds rather than the solvent. The moderate cytotoxic activity exhibited by the synthesized compounds suggests potential biological activity, with MAS-2 showing the most pronounced effect, possibly due to the presence of the dichlorophenyl moiety in its structure. These findings indicate that the compounds possess acceptable safety profiles at lower concentrations while maintaining measurable biological activity.

Chapter 5

Conclusion and Future Prospects

To conclude, this research has effectively demonstrated that combining synthetic organic chemistry with pharmacophore-based computational modeling is a powerful strategy for accelerating the discovery of novel inhibitors. The integration of in-silico screening with wet-lab synthesis led to the successful design and preparation of a promising candidate, referred to as MAS-1, MAS-2, MAS-3. This compound emerged as a potential lead molecule as NF-κB based on its favorable pharmacokinetic properties, including good solubility, permeability, and a low predicted toxicity profile. Most notably, MAS-3 fulfilled the critical criterion of blood-brain barrier (BBB) permeability, a major challenge in the development of central nervous system (CNS) drugs. This feature is particularly important for molecules targeting neurodegenerative conditions like Alzheimer's disease. The compound was synthesized through a carefully planned synthetic route and characterized using basic analytical techniques, including FTIR and NMR analysis. While these initial findings are promising, the true therapeutic value of MAS-1, MAS-2 and MAS-3 can only be confirmed through further biological evaluation. Planned in-vitro and in-vivo studies will be necessary to determine its actual inhibitory effect, mechanism of action, and overall safety profile. In summary, this study provides valuable insight into the utility of an integrated research approach that combines computational drug design with hands-on laboratory synthesis. It

sets a solid foundation for future work aimed at developing effective therapeutic agents against neuroinflammatory and neurodegenerative disorders.

5.1 Future Recommendations

To further advance this research, several key steps are recommended. Firstly, in-vitro NF-B inhibition assays should be carried out to experimentally verify the biological activity of the synthesized compounds and confirm their potential as NF-B inhibitors. This will provide direct evidence of the compounds' mechanism of action at the molecular level. Secondly, structure–activity relationship (SAR) optimization is essential to refine the chemical structures by introducing strategic modifications aimed at enhancing their potency, selectivity, and physicochemical stability. Such optimization could also help in reducing toxicity and improving target specificity. Thirdly, comprehensive in-vivo studies should be conducted using suitable animal models to evaluate the therapeutic efficacy of the lead compounds under physiological conditions. These studies must be accompanied by a detailed analysis of pharmacokinetic (PK) and pharmacodynamic (PD) parameters to assess drug absorption, distribution, metabolism, excretion, and the biological response over time. Lastly, extensive toxicological profiling of the SAR optimized compounds is necessary to ensure safety.

Bibliography

[1] A. Talevi, "Computer-aided drug design: An overview," in *Computational Drug Discovery and Design*, pp. 1–19, 2018.

[2] I. Kapetanovic, "Computer-aided drug discovery and development (caddd): in silico-chemico-biological approach," *Chemico-biological Interactions*, vol. 171, no. 2, pp. 165–176, 2008.

[3] A. Baldi, "Computational approaches for drug design and discovery: An overview," *Systematic Reviews in Pharmacy*, vol. 1, no. 1, p. 99, 2010.

[4] C. Choudhury and G. N. Sastry, "Pharmacophore modelling and screening: concepts, recent developments and applications in rational drug design," in *Structural Bioinformatics: Applications in Preclinical Drug Discovery Process*, pp. 25–53, 2019.

[5] P. Agnihotri *et al.*, "Anti-inflammatory potential of selective small compounds by targeting tnf- & nf-kb signaling: a comprehensive molecular docking and simulation study," *Journal of Biomolecular Structure and Dynamics*, vol. 41, no. 23, pp. 13815–13828, 2023.

[6] R. Ghosh, S. Roy, G. Rakshit, N. K. Singh, and N. J. Maiti, "Pharmacophore modeling in drug design," in *Computational Methods for Rational Drug Design*, pp. 167–194, 2025.

[7] M. N. da Rocha *et al.*, "Ligand and structure-based virtual screening approaches in drug discovery: minireview," *Molecular Diversity*, pp. 1–11, 2024.

[8] D. Mendez *et al.*, "Chembl: towards direct deposition of bioassay data," *Nucleic Acids Research*, vol. 47, no. D1, pp. D930–D940, 2019.

[9] J. D. Durrant and J. A. McCammon, "Molecular dynamics simulations and drug discovery," *BMC Biology*, vol. 9, pp. 1–9, 2011.

[10] Y. Li *et al.*, "Pharmacophore modeling, molecular docking and molecular dynamics simulations toward identifying lead compounds for chk1," *Computational Biology and Chemistry*, vol. 76, pp. 53–60, 2018.

[11] D. Giordano, C. Biancaniello, M. A. Argenio, and A. Facchiano, "Drug design by pharmacophore and virtual screening approach," *Pharmaceuticals*, vol. 15, no. 5, p. 646, 2022.

[12] O. Guner, "The impact of pharmacophore modeling in drug design," *IDrugs*, vol. 8, no. 7, p. 567, 2005.

[13] U. Shareef, A. Altaf, M. K. Zargaham, R. Bhatti, A. Ibrahim, and M. A. Zahid, "Ligand based pharmacophore modeling, virtual screening, molecular docking, molecular dynamic simulation and in-silico admet studies for the discovery of potential bace-1 inhibitors," 2023. Unpublished or preprint.

[14] N. E.-H. Daoud *et al.*, "Admet profiling in drug discovery and development: perspectives of in silico, in vitro and integrated approaches," *Current Drug Metabolism*, vol. 22, no. 7, pp. 503–522, 2021.

[15] M. Amelimojarad, M. Amelimojarad, and X. Cui, "The emerging role of brain neuroinflammatory responses in alzheimer's disease," *Frontiers in Aging Neuroscience*, vol. 16, p. 1391517, 2024.

[16] A. s. Association, "2019 alzheimer's disease facts and figures," *Alzheimer's & Dementia*, vol. 15, no. 3, pp. 321–387, 2019.

[17] Y. Chen and Y. Yu, "Tau and neuroinflammation in alzheimer's disease: interplay mechanisms and clinical translation," *Journal of Neuroinflammation*, vol. 20, no. 1, p. 165, 2023.

[18] W. J. Lukiw, "Nf-kb (p50/p65)-mediated pro-inflammatory microrna (mirna) signaling in alzheimer's disease (ad)," *Frontiers in Molecular Neuroscience*, vol. 15, p. 943492, 2022.

[19] X. Qing *et al.*, "Pharmacophore modeling: advances, limitations, and current utility in drug discovery," *Journal of Receptor, Ligand and Channel Research*, pp. 81–92, 2014.

[20] M. Iskar, G. Zeller, X.-M. Zhao, V. van Noort, and P. Bork, "Drug discovery in the age of systems biology: the rise of computational approaches for data integration," *Current Opinion in Biotechnology*, vol. 23, no. 4, pp. 609–616, 2012.

[21] A. Vuorinen and D. Schuster, "Methods for generating and applying pharmacophore models as virtual screening filters and for bioactivity profiling," *Methods*, vol. 71, pp. 113–134, 2015.

[22] S. L. Dixon, *Pharmacophore Methods*. University Press: Cambridge, 2010.

[23] O. F. Güner, *Pharmacophore Perception, Development, and Use in Drug Design*. Internat'l University Line, 2000.

[24] O. Guner, "History and evolution of the pharmacophore concept in computer-aided drug design," *Current Topics in Medicinal Chemistry*, vol. 2, no. 12, pp. 1321–1332, 2002.

[25] J. F. Blake and E. R. Laird, "Chapter 30. recent advances in virtual ligand screening," in *Unknown or Edited Volume*, 2003. Details incomplete, please verify source.

[26] H. A. Carlson *et al.*, "Developing a dynamic pharmacophore model for hiv-1 integrase," *Journal of Medicinal Chemistry*, vol. 43, no. 11, pp. 2100–2114, 2000.

[27] L. Kier, *Molecular Orbital Theory in Drug Research*. Elsevier, 2012.

[28] B. L. Jejurikar and S. H. Rohane, "Drug designing in discovery studio," 2021. Unpublished or technical document.

[29] K. Poptodorov, T. Luu, and R. D. Hoffmann, "Pharmacophore model generation software tools," in *Pharmacophores and Pharmacophore Searches*, vol. 32, pp. 15–47, 2006.

[30] S. A. Khedkar, A. K. Malde, E. C. Coutinho, and S. Srivastava, "Pharmacophore modeling in drug discovery and development: an overview," *Medicinal Chemistry*, vol. 3, no. 2, pp. 187–197, 2007.

[31] M. T. Muhammed and E. Akı-yalcın, "Pharmacophore modeling in drug discovery: methodology and current status," *Journal of the Turkish Chemical Society Section A: Chemistry*, vol. 8, no. 3, pp. 749–762, 2021.

[32] S. Y. Ugurlu, "Computational methods in drug discovery and development," 2024. Unpublished or in-press work.

[33] A. R. Leach and V. J. Gillet, *An Introduction to Chemoinformatics*. Springer, 2007.

[34] H. Zhao and A. Caflisch, "Molecular dynamics in drug design," *European Journal of Medicinal Chemistry*, vol. 91, pp. 4–14, 2015.

[35] S. L. Dixon, A. M. Smondyrev, and S. N. Rao, "Phase: a novel approach to pharmacophore modeling and 3d database searching," *Chemical Biology & Drug Design*, vol. 67, no. 5, pp. 370–372, 2006.

[36] A. M. E. Kerdawy, A. A. Osman, and M. A. Zaater, "Receptor-based pharmacophore modeling, virtual screening, and molecular docking studies for the discovery of novel gsk-3 inhibitors," *Journal of Molecular Modeling*, vol. 25, pp. 1–21, 2019.

[37] S. Ranganathan, K. Nakai, and C. Schonbach, *Encyclopedia of Bioinformatics and Computational Biology: ABC of Bioinformatics*. Elsevier, 2018.

[38] S. A. Hollingsworth and R. O. Dror, "Molecular dynamics simulation for all," *Neuron*, vol. 99, no. 6, pp. 1129–1143, 2018.

[39] V. D. Mouchlis, G. Melagraki, L. C. Zacharia, and A. Afantitis, "Computer-aided drug design of -secretase, -secretase and anti-tau inhibitors for the discovery of novel alzheimer's therapeutics," *International Journal of Molecular Sciences*, vol. 21, no. 3, 2020.

[40] R. Shukla and T. Tripathi, "Molecular dynamics simulation in drug discovery: opportunities and challenges," in *Innovations and Implementations of Computer Aided Drug Discovery Strategies in Rational Drug Design*, pp. 295–316, 2021.

[41] J. D. Durrant and J. A. McCammon, "Molecular dynamics simulations and drug discovery," *BMC Biology*, vol. 9, no. 1, pp. 1–9, 2011.

[42] S. Release, "Desmond molecular dynamics system, de shaw research, new york, ny, 2021. maestro-desmond interoperability tools, schrödinger," 2023. Software documentation.

[43] M. Hernández-Rodríguez, J. Correa-Basurto, A. Gutiérrez, J. Vitorica, and M. C. Rosales-Hernández, "Asp32 and asp228 determine the selective inhibition of bace1 as shown by docking and molecular dynamics simulations," *European Journal of Medicinal Chemistry*, vol. 124, pp. 1142–1154, 2016.

[44] P. Castleman, G. Szwabowski, D. Bowman, J. Cole, A. Parrill, and D. Baker, "Ligand-based g protein coupled receptor pharmacophore modeling: Assessing the role of ligand function in model development," *Journal of Molecular Graphics and Modelling*, vol. 111, p. 108107, 2022.

[45] P. Kaur, V. Sharma, and V. Kumar, "Pharmacophore modelling and 3d-qsar studies on n," *International Journal of Medicinal Chemistry*, vol. 2012, 2012.

[46] K. K. Reddy, S. K. Singh, N. Dessalew, S. K. Tripathi, and C. Selvaraj, "Pharmacophore modelling and atom-based 3d-qsar studies on n-methyl pyrimidones as hiv-1 integrase inhibitors," *Journal of Enzyme Inhibition and Medicinal Chemistry*, vol. 27, no. 3, pp. 339–347, 2012.

[47] H. Xie, K. Qiu, and X. Xie, "Pharmacophore modeling, virtual screening, and 3d-qsar studies on a series of non-steroidal aromatase inhibitors," *Medicinal Chemistry Research*, vol. 24, pp. 1901–1915, 2015.

[48] K. S. Bhadoriya, M. C. Sharma, and S. V. Jain, "Pharmacophore modeling and atom-based 3d-qsar studies on amino derivatives of indole as potent isoprenylcysteine carboxyl methyltransferase (icmt) inhibitors," *Journal of Molecular Structure*, vol. 1081, pp. 466–476, 2015.

[49] A. I. Foudah, A. A. Sallam, M. R. Akl, and K. A. E. Sayed, "Optimization, pharmacophore modeling and 3d-qsar studies of sipholanes as breast cancer migration and proliferation inhibitors," *European Journal of Medicinal Chemistry*, vol. 73, pp. 310–324, 2014.

[50] J. Kirchmair, P. Markt, S. Distinto, G. Wolber, and T. Langer, "Evaluation of the performance of 3d virtual screening protocols: Rmsd comparisons, enrichment assessments, and decoy selection—what can we learn from earlier mistakes?," *Journal of Computer-Aided Molecular Design*, vol. 22, pp. 213–228, 2008.

[51] J. D. Scott *et al.*, "Discovery of the 3-imino-1, 2, 4-thiadiazinane 1, 1-dioxide derivative verubecestat (mk-8931)–a -site amyloid precursor protein cleaving enzyme 1 inhibitor for the treatment of alzheimer's disease," 2016. Conference or technical report; complete citation needed.

[52] G. Wolber and T. Langer, "Ligandscout: 3-d pharmacophores derived from protein-bound ligands and their use as virtual screening filters," *Journal of Chemical Information and Modeling*, vol. 45, no. 1, pp. 160–169, 2005.

[53] S. F. Sousa, P. A. Fernandes, and M. J. Ramos, "Protein–ligand docking: current status and future challenges," *Proteins: Structure, Function, and Bioinformatics*, vol. 65, no. 1, pp. 15–26, 2006.

[54] N. J. Richmond, C. A. Abrams, P. R. Wolohan, E. Abrahamian, P. Willett, and R. D. Clark, "Galahad: 1. pharmacophore identification by hypermolecular alignment of ligands in 3d," *Journal of Computer-Aided Molecular Design*, vol. 20, pp. 567–587, 2006.

[55] J. Varady *et al.*, "Molecular modeling of the three-dimensional structure of dopamine 3 (d3) subtype receptor: discovery of novel and potent d3 ligands through a hybrid pharmacophore-and structure-based database searching approach," *Journal of Medicinal Chemistry*, vol. 46, no. 21, pp. 4377–4392, 2003.

[56] S. Pal *et al.*, "Ligand-based pharmacophore modeling, virtual screening and molecular docking studies for discovery of potential topoisomerase i inhibitors," *Computational and Structural Biotechnology Journal*, vol. 17, pp. 291–310, 2019.

[57] X.-Y. Meng, H.-X. Zhang, M. Mezei, and M. Cui, "Molecular docking: a powerful approach for structure-based drug discovery," *Current Computer-Aided Drug Design*, vol. 7, no. 2, pp. 146–157, 2011.

[58] A. Sethi, K. Joshi, K. Sasikala, and M. Alvala, "Molecular docking in modern drug discovery: Principles and recent applications," in *Drug Discovery and Development—New Advances*, vol. 2, pp. 1–21, 2019.

[59] T. M. Menchaca, C. Juárez-Portilla, and R. C. Zepeda, "Past, present, and future of molecular docking," in *Drug Discovery and Development—New Advances*, 2020.

[60] O. M. Salo-Ahen *et al.*, "Molecular dynamics simulations in drug discovery and pharmaceutical development," *Processes*, vol. 9, no. 1, p. 71, 2020.

[61] K. Hacker, "The burden of chronic disease," *Mayo Clinic Proceedings: Innovations, Quality & Outcomes*, vol. 8, no. 1, pp. 112–119, 2024.

[62] G. Livingston *et al.*, "Dementia prevention, intervention, and care: 2024 report of the lancet standing commission," *The Lancet*, vol. 404, no. 10452, pp. 572–628, 2024.

[63] M. A. DeTure and D. W. Dickson, "The neuropathological diagnosis of alzheimer's disease," *Molecular Neurodegeneration*, vol. 14, no. 1, p. 32, 2019.

[64] C. R. J. Jr *et al.*, "Nia-aa research framework: toward a biological definition of alzheimer's disease," *Alzheimer's & Dementia*, vol. 14, no. 4, pp. 535–562, 2018.

[65] S. Evans-Lacko, E. Aguzzoli, S. Read, A. Comas-Herrera, and N. Farina, "World alzheimer report 2024: Global changes in attitudes to dementia," tech. rep., Alzheimer's Disease International, London, United Kingdom, 2024.

[66] J. Guo *et al.*, "The disease burden, risk factors and future predictions of alzheimer's disease and other types of dementia in asia from 1990 to 2021," *The Journal of Prevention of Alzheimer's Disease*, vol. 12, no. 5, p. 100122, 2025.

[67] A. Zaidi *et al.*, "Understanding, beliefs and treatment of dementia in pakistan," 2019. Unpublished report.

[68] S. Balouch, A. Zaidi, N. Farina, and R. Willis, "Dementia awareness, beliefs and barriers among family caregivers in pakistan," *Dementia*, vol. 20, no. 3, pp. 899–918, 2021.

[69] S. Chen *et al.*, "The global macroeconomic burden of alzheimer's disease and other dementias: estimates and projections for 152 countries or territories," *The Lancet Global Health*, vol. 12, no. 9, pp. e1534–e1543, 2024.

[70] J. F. Trani *et al.*, "Multidimensional poverty increases dementia risk in south africa, afghanistan, and pakistan among adults age 50 and older," *Alzheimer's & Dementia*, vol. 19, p. e082882, 2023.

[71] D. J. Selkoe and J. Hardy, "The amyloid hypothesis of alzheimer's disease at 25 years," *EMBO Molecular Medicine*, vol. 8, no. 6, pp. 595–608, 2016.

[72] M. T. Heneka, D. T. Golenbock, and E. Latz, "Innate immunity in alzheimer's disease," *Nature Immunology*, vol. 16, no. 3, pp. 229–236, 2015.

[73] R. H. Swerdlow, "Mitochondria and mitochondrial cascades in alzheimer's disease," *Journal of Alzheimer's Disease*, vol. 62, no. 3, pp. 1403–1416, 2018.

[74] R. T. Bartus, R. L. D. III, B. Beer, and A. S. Lippa, "The cholinergic hypothesis of geriatric memory dysfunction," *Science*, vol. 217, no. 4558, pp. 408–414, 1982.

[75] B. V. Zlokovic, "Neurovascular pathways to neurodegeneration in alzheimer's disease and other disorders," *Nature Reviews Neuroscience*, vol. 12, no. 12, pp. 723–738, 2011.

[76] N. M. Vogt *et al.*, "Gut microbiome alterations in alzheimer's disease," *Scientific Reports*, vol. 7, no. 1, p. 13537, 2017.

[77] T. Wang, Y. Liu, Y. Lu, and L. Chi, "Ntn-1 attenuates amyloid--mediated microglial neuroinflammation and memory impairment via the nf-b pathway and nlrp3 inflammasome in a rat model of alzheimer's disease," *Frontiers in Aging Neuroscience*, vol. 17, p. 1516399, 2025.

[78] B. Kaltschmidt, N. J. Czaniera, W. Schulten, and C. Kaltschmidt, "Nf-b in alzheimer's disease: Friend or foe? opposite functions in neurons and glial cells," *International Journal of Molecular Sciences*, vol. 25, no. 21, p. 11353, 2024.

[79] Z. Breijyeh and R. Karaman, "Comprehensive review on alzheimer's disease: causes and treatment," *Molecules*, vol. 25, no. 24, p. 5789, 2020.

[80] E. Lee and Y. Chang, "Modulating neuroinflammation as a prospective therapeutic target in alzheimer's disease," *Cells*, vol. 14, no. 3, p. 168, 2025.

[81] D. Melchiorri, S. Merlo, B. Micallef, J.-J. Borg, and F. Dráfi, "Alzheimer's disease and neuroinflammation: will new drugs in clinical trials pave the way to a multi-target therapy?," *Frontiers in Pharmacology*, vol. 14, p. 1196413, 2023.

[82] Y. Verma, H. Sachdeva, S. Kalra, P. Kumar, and G. Singh, "Unveiling the complex role of nf-b in alzheimer's disease: Insights into brain inflammation and potential therapeutic targets," *Georgian Medical News*, vol. 342, pp. 133–141, 2023.

[83] X. Shan *et al.*, "Recent insights on the role of nuclear receptors in alzheimer's disease: Mechanisms and therapeutic application," *International Journal of Molecular Sciences*, vol. 26, no. 3, p. 1207, 2025.

[84] C. He *et al.*, "Qi fu yin ameliorates neuroinflammation through inhibiting rage and tlr4/nf-b pathway in ad model rats," *Aging (Albany NY)*, vol. 15, no. 22, p. 13239, 2023.

[85] D. C. Blakemore *et al.*, "Organic synthesis provides opportunities to transform drug discovery," *Nature Chemistry*, vol. 10, no. 4, pp. 383–394, 2018.

[86] G. AMEEN, *Advances in organic chemistry*. CHEMISTRY: THE MODERN APPROACH, 2024.

[87] W. Parys, M. Dołowy, and A. Pyka-Pajak, "Significance of chromatographic techniques in pharmaceutical analysis," *Processes*, vol. 10, no. 1, p. 172, 2022.

[88] Y. Zhang and A. K. Ray, "Liquid–liquid extraction," in *Coulson and Richardson's Chemical Engineering*, pp. 257–312, Elsevier, 2023.

[89] S. H. Yalkowsky and D. Alantary, "Estimation of melting points of organics," *Journal of Pharmaceutical Sciences*, vol. 107, no. 5, pp. 1211–1227, 2018.

[90] Z. Dai, L. Wang, X. Lu, and X. Ji, "Melting points of ionic liquids: Review and evaluation," *Green Energy & Environment*, vol. 9, no. 12, pp. 1802–1811, 2024.

[91] Y. Song, Y. Cong, B. Wang, and N. Zhang, "Applications of fourier transform infrared spectroscopy to pharmaceutical preparations," *Expert Opinion on Drug Delivery*, vol. 17, no. 4, pp. 551–571, 2020.

[92] M. N. Dole, P. A. Patel, S. D. Sawant, and P. S. Shedpure, "Advance applications of fourier transform infrared spectroscopy," *International Journal of Pharmaceutical Sciences Review and Research*, vol. 7, no. 2, pp. 159–166, 2011.

[93] J. Keeler, *Understanding NMR spectroscopy*. John Wiley & Sons, 2011.

[94] T. D. Claridge, *High-resolution NMR techniques in organic chemistry*. Elsevier, 2016.

[95] G. C. Roberts, "Applications of nmr in drug discovery," *Drug Discovery Today*, vol. 5, no. 6, pp. 230–240, 2000.

[96] Q. Li and C. Kang, "A practical perspective on the roles of solution nmr spectroscopy in drug discovery," *Molecules*, vol. 25, no. 13, p. 2974, 2020.

[97] A. M. Davis and R. J. Riley, "Predictive admet studies, the challenges and the opportunities," *Current Opinion in Chemical Biology*, vol. 8, no. 4, pp. 378–386, 2004.

[98] O. K. Alhmoudi, M. Aboushanab, M. Thameem, A. Elkamel, and A. A. AlHammadi, "Domain adaptation of a smiles chemical transformer to selfies with limited computational resources," *Scientific Reports*, vol. 15, no. 1, p. 23627, 2025.

[99] Schrödinger, "Schrödinger release 2023-3: Maestro, schrödinger, llc, new york, ny," 2023.

[100] S. Wetzel *et al.*, "Interactive exploration of chemical space with scaffold hunter," *Nature Chemical Biology*, vol. 5, no. 8, pp. 581–583, 2009.

[101] T. Zhu *et al.*, "A comparison of scaffold decomposition with clustering methods in compound set enrichment to identify latent chemical series in high-throughput screening." Unpublished / No year provided.

[102] L. Schrodinger, "Schrödinger release 2023-3: Ligprep, schrödinger, llc, new york, ny," 2023.

[103] S. Epik, "Schrödinger release 2023-3: Epik, schrödinger, llc, new york, ny," 2023.

[104] J. C. Shelley, A. Cholleti, L. L. Frye, J. R. Greenwood, M. R. Timlin, and M. Uchimaya, "Epik: a software program for pk_a prediction and protonation state generation for drug-like molecules," *Journal of Computer-Aided Molecular Design*, vol. 21, pp. 681–691, 2007.

[105] S.-Y. Yang, "Pharmacophore modeling and applications in drug discovery: challenges and recent advances," *Drug Discovery Today*, vol. 15, no. 11-12, pp. 444–450, 2010.

[106] M. M. Mysinger, M. Carchia, J. J. Irwin, and B. K. Shoichet, "Directory of useful decoys, enhanced (dud-e): better ligands and decoys for better benchmarking," *Journal of Medicinal Chemistry*, vol. 55, no. 14, pp. 6582–6594, 2012.

[107] L. Piccagli *et al.*, "Docking of molecules identified in bioactive medicinal plants extracts into the p50 nf-kappab transcription factor: correlation with inhibition of nf-kappab/dna interactions and inhibitory effects on il-8 gene expression," *BMC Structural Biology*, vol. 8, pp. 1–13, 2008.

[108] P. P. W. Schrödinger, "Schrödinger release 2023-3: Protein preparation wizard; epik, schrödinger, llc, new york, ny, 2023; impact, schrödinger, llc, new york, ny; prime, schrödinger, llc, new york, ny, 2023," 2023.

[109] U. Manual, "Schrödinger release 2019–3: Glide, schrödinger, llc, new york, ny," 2018.

[110] R. A. Friesner *et al.*, "Glide: a new approach for rapid, accurate docking and scoring. 1. method and assessment of docking accuracy," *Journal of Medicinal Chemistry*, vol. 47, no. 7, pp. 1739–1749, 2004.

[111] P. Schrödinger, "Schrödinger release 2023-3: Prime, schrödinger, llc, new york, ny," 2023.

[112] M. P. Jacobson *et al.*, "A hierarchical approach to all-atom protein loop prediction," *Proteins: Structure, Function, and Bioinformatics*, vol. 55, no. 2, pp. 351–367, 2004.

[113] S. Genheden and U. Ryde, "The mm/pbsa and mm/gbsa methods to estimate ligand-binding affinities," *Expert Opinion on Drug Discovery*, vol. 10, no. 5, pp. 449–461, 2015.

[114] J. Li, R. Abel, K. Zhu, Y. Cao, S. Zhao, and R. A. Friesner, "The vsgb 2.0 model: a next generation energy model for high resolution protein structure modeling," *Proteins: Structure, Function, and Bioinformatics*, vol. 79, no. 10, pp. 2794–2812, 2011.

[115] G. J. Martyna, D. J. Tobias, and M. L. Klein, "Constant pressure molecular dynamics algorithms," *The Journal of Chemical Physics*, vol. 101, no. 5, pp. 4177–4189, 1994.

[116] A. Leggio *et al.*, "One-pot synthesis of amides from carboxylic acids activated using thionyl chloride," *RSC Advances*, vol. 6, no. 41, pp. 34468–34475, 2016.

[117] M. R. Hamidi, B. Jovanova, and T. K. Panovska, "Toxicological evaluation of the plant products using brine shrimp (artemia salina l.) model," *Macedonian Pharmaceutical Bulletin/Makedonsko Farmacevtski Bilten*, vol. 60, no. 1, 2014.

[118] Q. S. Sarah, F. C. Anny, and M. Misbahuddin, "Brine shrimp lethality assay," *Bangladesh Journal of Pharmacology*, vol. 12, no. 2, pp. 186–189, 2017.

[119] A. Tsakni *et al.*, "In vitro determination of antimicrobial, antioxidant and antiviral properties of greek plant extracts," *Microorganisms*, vol. 13, no. 1, p. 177, 2025.

[120] Gulcin and S. H. Alwasel, "Dpph radical scavenging assay," *Processes*, vol. 11, no. 8, p. 2248, 2023.

[121] M. S. Rana *et al.*, "Antioxidant activity of schiff base ligands using the dpph scavenging assay: an updated review," *RSC Advances*, vol. 14, no. 45, pp. 33094–33123, 2024.

[122] M. Hatami, M. Mortazavi, Z. Baseri, B. Khani, M. Rahimi, and S. Babaei, "Antioxidant compounds in the treatment of alzheimer's disease: Natural, hybrid, and synthetic products," *Evidence-Based Complementary and Alternative Medicine*, vol. 2023, no. 1, p. 8056462, 2023.